North Carolina Agricultural and Technical State University
Aggie Digital Collections and Scholarship

Dissertations | Electronic Theses and Dissertations

2012

Modeling And Optimal Mitigation Of Impulsive Low Frequency

Meng Vang
North Carolina Agricultural and Technical State University

Follow this and additional works at: https://digital.library.ncat.edu/dissertations

Recommended Citation

Vang, Meng, "Modeling And Optimal Mitigation Of Impulsive Low Frequency" (2012). *Dissertations*. 23.
https://digital.library.ncat.edu/dissertations/23

This Dissertation is brought to you for free and open access by the Electronic Theses and Dissertations at Aggie Digital Collections and Scholarship. It has been accepted for inclusion in Dissertations by an authorized administrator of Aggie Digital Collections and Scholarship. For more information, please contact iyanna@ncat.edu.

MODELING AND OPTIMAL MITIGATION OF IMPULSIVE LOW-FREQUENCY OUTDOOR NOISE

by

Meng Vang

A dissertation submitted to the graduate faculty
in partial fulfillment of the requirements for the degree of
DOCTOR OF PHILOSOPHY

Department: Electrical Engineering
Major: Electrical Engineering
Major Professor: Dr. Marwan Bikdash

North Carolina A&T State University
Greensboro, North Carolina
2012

ABSTRACT

Vang, Meng. MODELING AND OPTIMAL MITIGATION OF IMPULSIVE LOW-FREQUENCY OUTDOOR NOISE. (**Major Advisor: Marwan Bikdash**), North Carolina Agricultural and Technical State University.

Low-frequency outdoor noise is very common in urban environments and can propagate over long distances. Residents living in the vicinity of a military base and other noisy areas often are annoyed by this noise. Most of the theoretical and experimental work that have been done to study and reduce this type of noise involved the use of barriers and sound proofing the residential houses. The attenuation of acoustic waves propagating above hard surfaces over long distances depends on the shape of the surface. Therefore, the landscape is a factor in combating outdoor noise. In this dissertation, an anti-propagation approach involving the use of corrugated surfaces or sinusoidally shaped berms to suppress outdoor noise was proposed.

Finite element analysis and the equivalent source method (ESM) were employed to investigate the effects of corrugated surfaces on the acoustic transmission loss. The equivalent source method (ESM) was used to model different surface geometries and employed in conjunction with a nonlinear optimization algorithm to compute the surface shape that will result in the most acoustic loss. The corrugation method was shown to be effective against certain frequencies and can be used to combat low-frequency outdoor noise.

School of Graduate Studies
North Carolina Agricultural and Technical State University

This is to certify that the Doctoral Dissertation of

Meng Vang

has met the dissertation requirements of
North Carolina Agricultural and Technical State University

Greensboro, North Carolina
2012

Approved by:

Dr. Marwan Bikdash Major Professor	Dr. Jung H. Kim Committee Member
Dr. Mannur Sundaresan Committee Member	Dr. Abdollah Homaifar Committee Member
Dr. Robert Li Committee Member	Dr. John Kelly Department Chairperson

Dr. Sanjiv Sarin
Associate Vice Chancellor for Research
and Dean of Graduate Studies

DEDICATION

This work is dedicated to my father and mother.

BIOGRAPHICAL SKETCH

Meng Vang was born on February 4, 1979 in Vinai, Thailand. He received his Bachelor of Science degree in Electrical and Computer Engineering from North Carolina State University in 2002. He received the Master of Science degree from the Department of Electrical and Computer Engineering at the North Carolina Agricultural and Technical State University in 2005. He is a candidate for a Ph.D. in the Department of Electrical and Computer Engineering at the North Carolina Agricultural and Technical State University.

ACKNOWLEDGEMENTS

I would thank my parents, Lee Vang and Song Lee, for their support and providing me with the motivation to pursue the Ph.D. degree.

I would like to sincerely thank Dr. Marwan Bikdash for his excellent guidance and support for which this dissertation would not have been possible without it. I would like to express my thanks to all of the committee members: Dr. Abdollah Homaifar, Dr. Robert Li, Dr. Mannur Sundaresan and Dr. Jung H. Kim. I also would like thank Dr. Numan Dogan and Dr. Michelle Swearingen for the guidance they have provided.

I wish to thank Dr. Prabhat Ranjan Pathak, Dr. Satish Tadiparthi, Dr. Serap Karagol and all of the members of the Advanced Robotics Laboratory for their advice and encouragement.

This dissertation has been supported by the Army Construction Engineering Research Laboratory (CERL) under contracts W1932T-06-0089 and W9132T-07-P-0172. I appreciate their support.

TABLE OF CONTENTS

LIST OF FIGURES

FIGURES **PAGE**

LIST OF TABLES

TABLES **PAGE**

CHAPTER 1
INTRODUCTION

As the number of airplanes, trains, and highways continues to increase, the noise level of our cities and environment continues to rise. In addition to noise produced by civilians, there are those that are produced by the military. These noises are generated by gunfire, explosions, artillery fires, and military vehicles such as airplanes, tanks, and personnel carrier vehicles. Noises generated by the military can be heard up to several kilometers away, particularly those produced by explosions which have a strong low-frequency content and can travel over long distances. As a result, military bases are a source of annoyance to civilian residents including those residing several kilometers away. The pervasive nature of low-frequency noise also presents many acoustic problems to the architects, designers, planners and engineers.

This research focuses on low-frequency outdoor noise and addresses some of the problems associated with it. The following are proposed: 1) a method to suppress outdoor low-frequency noise, 2) a method to model the effects undulating surfaces on the acoustic energy loss, 3) using perturbation theory to reducing acoustic energies and 4) an algorithm to optimize the acoustic loss.

1.1 Impulsive Noise

One can think of an impulsive noise as an unwanted instantaneous sharp sound. Examples of impulsive noise include that produced by explosions and gunfire. Most of

the energy associated with impulsive noise is located at the low-frequency (20-50 Hz) end of the energy spectrum. Moreover, low-frequency noise propagates efficiently. Hence, residential houses many kilometers away are affected. Other structures, particularly those with a low resonant frequency, such as windows, tables, plates etc. vibrate or rattle as a result of their interaction with low-frequency noise.

To gain a better understanding of this phenomenon, one has to look at the characteristic waveform of the explosion or the source of the noise, its propagation characteristics and attenuation in the atmosphere, and the interaction between the low-frequency noise and structures.

Baker [1] discussed the phenomenology of explosion in air and air blast theory. In his book, he also discussed methods of computation and blast experimentation as well as providing curves and tables of compiled blast parameters. Some experimental data and graphs were also provided by Baker making his book an invaluable resource for this research. Bangash [2] has similar details in his book. Bangash also presents a comprehensive study of the structural dynamics of impact and explosion by providing a survey of types of aircraft, missiles, bombs and detonators. Additionally, he included empirical models developed for different materials, water surfaces, soil and rock medium. His book is very useful when studying the interaction between blast waves and structures.

In 1993, Ford et al. [3] measured the pressure waveform from small unconfined charges of plastic explosive. In their experiment, the pressure waveforms were measured in free air from unconfined 125-g and 1-kg charges of plastic explosive at distances of 1000 m. They concluded that propagation over concrete and water has similar waveforms while

propagation over grass has much of the high frequency content removed resulting in a different waveform. There are also numerous studies conducted on underwater explosions.

There also had been numerous studies on the propagation of acoustic waves in air. Reed [4], in 1977, looked at atmospheric attenuation rate of an explosion wave. Reed discussed various attenuation factors and relationships to frequency to the total wave pressure signature of an explosion wave, both positive and negative phases. He concluded that sound attenuation have shown an attenuation factor approximately dependent on the five-fourths power of frequency, rather than the square. This new factor gives faster attenuation that is probably caused by a combination of molecular relaxation with small-scale inhomogeneities and turbulence usually present in the real atmosphere. Reed also provided explosion-wave signatures for different attenuation scenarios. These signatures have been used in some of the simulations in our research.

Downing et al. [5] did a study on the measurement and prediction of nonlinearity of outdoor propagation of periodic signals. They argued that there are limited numbers of experiments dedicated to the measurement of finite-amplitude effects in outdoor continuous-wave sound propagation. Two particular papers were mentioned. One by Theobald called "Experimental study of outdoor propagation of spherically spreading periodic acoustic waves of finite amplitude" and the other by Webster and Blackstock called "Experimental investigation of outdoor propagation of finite-amplitude noise." These two particular papers were mentioned because both studies "showed clear evidence of nonlinear propagation in that the measured high frequency sound pressure levels were significantly greater than those predicted with linear theory." Authors' purpose was to discuss their experimen-

tal results that show evidence of nonlinear effects. In their experiment, the U.S. Army Research Laboratory's Mobile Acoustic Source or MOAS was used to generate the high-amplitude periodic signals. Several microphones (Bruel and Kjaer Type 4190) were placed at various distances and heights to measure the signals. The authors used a nonlinear numerical model based on the generalized Burgers equation (GBE) to compare against their field experiment. The result of the comparison showed that the mean absolute error was significantly less for the nonlinear model than the linear model for most cases.

In 1988, Walkden and West [6] used a ray tube approach to predict atmospheric acoustic propagation. The ray tubes, each consisting of a group of four rays surrounding a central ray, are launched from an initial surface close to the source. The ray tube methods have two components. One is the ray path calculation and the other is the prediction of pressure levels along elementary ray tubes formed from a set of neighboring rays. Comparisons show that reasonable agreement between predictions and measurements is obtained in enhancement regions. However, prediction of sound levels will not be useful in regions where rays cross or which are close to a shadow boundary. Additionally, predictions are limited to frequencies high enough for the geometric ray acoustic approximations to apply.

While it is meaningful to understand the source of the noise and how noise propagates, it is also important to understand what happens at the interface where the sound wave meets a structure such as a wall. Sound and structure interaction is an interesting phenomenon. There are numerous studies in this area as well. In 1963, Lyon [7] studied noise reduction of rectangular enclosures with one flexible wall. Lyon computed the noise reduction for very low frequencies where both wall and enclosed volume are stiffness-controlled,

for frequencies where the wall is resonant and the volume is stiff, and for frequencies where both the wall and the acoustic space have resonant behavior. In 1966, Morse [8] looked at the transmission of sound through a circular membrane in a plane wall. The actual setup involved a plane, rigid wall having a circular window, across which is stretched a membrane under tension, in contact with an acoustic medium on both sides. One side of the wall was excited by a plane wave. Morse derived formulas for the total power transmitted through the membrane and for the distribution in angle of the transmitted wave.

To gain a better understanding of the structural-acoustic coupling mechanism, Kim and Kim studied structural-acoustic coupling using a partially opened plate-cavity [9]. Their goal was to understand the coupling mechanism of a generally coupled system that has direct interaction between a finite interior fluid and a semi-infinite exterior one. The coupled system was excited by a source at a wall of the cavity. The behavior of the cavity is affected by the plate and the exterior acoustic field which is constructed by the energy going out through the plate and the hole. Kim and Kim [9] found out that the frequency characteristics are totally dependent on the properties of the plate, especially at the low frequency region where the cavity mode does not occur. They used near field acoustic holography to estimate sound field variables such as pressure and intensities and found out that there are two types of coupling mechanisms depending on the frequency and wavelength. One mechanism is when the plate and the cavity are strongly coupled. When this happens, the plate acts as a source. The second mechanism is where the coupling interaction behavior decreases the radiation efficiency. Kim and Kim [9] indicated that the frequencies

that determine whether the plate is good or bad radiator are found to be around the natural frequencies of the plate.

In 1988, Schomer and Averbuch did a study on indoor human response to blast sounds that generate rattle [10]. The authors had two objectives: to systematically test subjective response to the presence or absence of rattles in otherwise similar blast sound environments and to test if there were structural changes that could reduce annoyance within the indoor blast environment. Their tests were done using a specifically constructed test house and highly repeatable shake table to simulate the blast sounds. When the shake table was used as a giant loudspeaker, it generates a blast type waveform and achieves a peak, flat-weighted sound pressure level at the face of the building of up to 123 dB. To reduce the annoyance, the main wall of the house was stiffened. However, Schomer and Averbuch found that the stiffening of the main wall does not reduce the resulting blast noise annoyance.

In 1990, Schomer et al. [11] used the methods of paired-comparison testing with panels of subjects to determined the acoustical benefits of improved, blast noise reducing retrofit windows. Two houses were used in their study. House one received new, retrofit windows while house two remained with older windows. C-4 plastic explosives were set off approximately 1.2 km away from the houses. Loud speakers were placed in each house to produce white noise. They concluded that the retrofit windows are highly effective in providing enhanced sound isolation for blast noise. The data clearly show that the windows provide about a 14 dB improvement in terms of annoyance.

It is also important to understand how blast waves propagate around corners of houses. Most houses have 90 degree angle corners. In 2006, Liu and Albert [12] investigated sound propagation around a right-angle wall. In their experiment, they used small explosions (C4 explosives) as the source of their acoustic waves. A concrete wall 3.5 m high and 9.4 m long was constructed and pressure sensors were placed near and on the wall. Their experiment concluded that "diffraction acts as a low-pass filter on acoustic waveforms in agreement with simple diffraction theory, reducing the peak pressure and broadening the waveform shape received by a sensor in the shadow zone." The authors [12] also developed a fast two-dimensional finite difference time domain (FDTD) model to provide more insight into the propagation around the wall.

1.2 Abatement Methods

Residents living near military bases or highways are constantly exposed to noise. The noise impact can vary greatly from a nuisance to adverse effects on a person's health [13]. It is generally important to find an effective method to suppress outdoor noise. Over the past several decades, many have investigated different methods to combat outdoor noise including the use of barriers, screens and replacing residential house windows with noise resistant windows [14-18]. Alternate suppression method such as using the contour of the landscape as an anti-propagation tool has also been studied [19].

Some work had been done on the effects of corrugated surfaces on propagating acoustic waves. Most work involved wave propagating in waveguides, and only a few had considered undulating landscapes as a method to suppress outdoor noise. It is possible that

a corrugated surface can stop certain frequencies as shown by Kundu and et al. [20] who have investigated wave propagation in a corrugated waveguide and observed stop bands and pass bands. To target specific frequencies for elimination, one would have to consider the wavelength and amplitude of the corrugation. It can be difficult to find the exact shape of a surface that would reduce a specific range of frequencies. To help solve this problem, we need to be able to model the effects of outdoor surfaces.

Although the effects of corrugated surfaces can be modeled using finite element analysis, the computational cost can be tremendous especially when a detailed model is combined with a semi-infinite domain. In this study, we propose an alternative way to model the effects of outdoor hard surfaces on acoustic waves using equivalent sources. This method is implemented and simulated using Matlab. While the equivalent source method has been investigated by various researchers [21, 22], our investigation focused on the acoustic loss over various surface shapes.

1.3 Synopsis

The acoustic theories and boundary conditions are discussed in Chapter 2. In Chapter 3, the method of suppressing low-frequency outdoor noise using sinusoidally shaped surfaces is described and simulation results are presented. The simulations in Chapter 3 were conducted using Comsol Multiphysics, a finite element analysis and simulation software. Chapter 4 introduces the equivalent source method (ESM) and describes the utilization of ESM to model acoustically rigid surfaces. In this dissertation, simulations involving ESM were completed using Matlab. In Chapter 5, a method to change the geometry of a

surface using ESM and perturbation is presented. Chapter 6 employs the least squares method to estimate the amplitude of the equivalent sources. In Chapter 7, a method to optimize the acoustic loss is presented.

CHAPTER 2

THEORETICAL BACKGROUND

This chapter reviews the theories that are employed in this dissertation. Acoustic wave propagation can be described by the hyperbolic partial differential equation known as the wave equation. This equation is discussed in section 2.1. The wave equation is a function of two quantities, time and space and can be separated using the separation of variable method. Using this method, the wave equation can be simplified into Helmholtz equation. This is covered in section 2.2. The blast wave characteristic waveform is shown in section 2.3. Various boundary conditions are used in finite element analysis. These conditions are discussed in section 2.4.

2.1 The Wave Equation

The propagation of waves can be described by the wave equation. The wave equation is a partial differential equation that is derived using the equation of state, the continuity equation and the equation of motion. The wave equation is stated as

$$\nabla^2 p(r) = \frac{1}{c^2}\frac{\partial^2 p(r)}{\partial t^2} \tag{2.1}$$

where p is the pressure, t is time and r is the three dimensional Cartesian position vector. The solution for a given freqency, ω, and wavenumber, k, to Equation (2.1) has the form

$$p(r) = Ae^{\mathbf{j}(\omega t - kr)} \tag{2.2}$$

where A is the amplitude, ω is the angular frequency, k is the wavenumber, c is the speed of sound and r is the distance from the source. The angular frequency and wavenumber are defined by the equations

$$\omega = 2\pi f \tag{2.3}$$

$$k = \frac{\omega}{c}. \tag{2.4}$$

2.2 Helmholtz Equation

The separation of variable method can be applied to Equation (2.1) to separate the spatial term from the temporal term. Thus, the wave equation can be simplified as a time-independent equation by assuming time-harmonic dependence. This leads to the Helmholtz equation, and it is used extensively by COMSOL to describe its simulation. The Helmholtz equation is given in the form of

$$\nabla^2\phi + k^2\phi = 0$$

where c is the speed of sound, and ϕ is a spatial function defined on three-dimensional Euclidean space.

2.3 Impulsive Noise Waveform

When an explosion occurs, the pressure rises almost instantaneously above the ambient pressure then drops to a partial vacuum. The pressure will eventually return to the ambient pressure. This phenomenon is discussed by Ford et al. [3] and can be described

by the equation

$$p(t) = p_0 + p_s \left(1 - \frac{t}{\tau}\right) e^{-\frac{t}{\tau}}. \tag{2.5}$$

where t is time, τ is the positive phase duration, p_0 is the ambient pressure and p_s is the peak value of the pressure at the arrival time.

2.4 Boundary Conditions

Outdoor acoustic waves propagating over a hard surface can be modeled with just one domain and two boundary conditions. There are three types of boundary conditions that are used extensively in acoustic modeling. These boundary conditions are sound-hard (acoustically rigid), continuity and radiation boundary conditions. The sound-hard boundary condition is discussed in section 2.4.1. Sections 2.4.2 and 2.4.3 discuss the continuity and radiation boundary conditions respectively. Other boundary conditions include sound-soft, which is appropriate approximation for liquid-gas interface and impedance boundary conditions which is a generalization of the sound-hard and sound-soft boundary conditions are not used since the models do not have any interface of this type.

2.4.1 Sound-Hard Boundary Condition

When sound waves are being transmit from one medium to another, the amount of energy transmitted and reflected back are largely determined by the impedances of the two materials. If the impedance of the second medium is much larger than that of the first medium, then most of the energy is reflected. Likewise, if both media have roughly the same impedance then most of the energy is transmitted into the second medium. The two media that appear frequently in this dissertation are air and a solid such a concrete or

brick. The latter medium has a very large impedance and is rigid. A sound-hard boundary condition is used to model rigid surfaces. It is a condition in which the normal component of the particle velocity vanishes. The sound-hard boundary condition is given as

$$\left(\frac{1}{\rho}(\nabla p - \mathbf{q})\right) \cdot \overrightarrow{n} = 0 \tag{2.6}$$

where $\mathbf{q}$ is the source, p is the pressure, ρ is the density and $\overrightarrow{n}$ is the vector normal to the surface. If the medium has a constant density, and there is no source on the surface then Equation (2.6) is reduced to

$$\nabla p \cdot \overrightarrow{n} = 0. \tag{2.7}$$

2.4.2 Continuity Boundary Condition

When modeling acoustic wave propagation using finite element analysis software such as Comsol Multiphysics, there are often multiple domains that waves propagate through. These domains may consist of the same material in which waves will transmit from one domain to another without any reflections or different materials which could result in reflections. Whatever the case may be, when acoustic waves propagating from one domain to another, there is a continuity of the normal acceleration at the interface. The boundary where the two domains are touching is considered an interior boundary. The continuity of the normal acceleration can be modeled by using the continuity condition which can be written as,

$$\left[-\frac{1}{\rho_0}(\nabla p - \mathbf{q})_1\right] \cdot \overrightarrow{n} = \left[-\frac{1}{\rho_0}(\nabla p - \mathbf{q})_2\right] \cdot \overrightarrow{n} \tag{2.8}$$

where the subscript 1 and 2 represent domain 1 and 2.

2.4.3 Radiation Boundary Condition

Most of the explosion sound energy is radiated high into the atmosphere. This phenomenon complicates the simulation since it corresponds to a semi-infinite domain. Even though we are mostly interested in the propagation of acoustic waves near the surface of the ground and their impact on an area of interest, inaccurate implementation of the radiation term will invalidate the results.

To model an infinite or semi-infinite domain, it is appropriate to use the radiation boundary condition because it allows an outgoing wave to leave the modeling domain with very little or no reflection. The radiation boundary condition is one of the two absorbing boundary conditions available in COMSOL Multiphysics The other absorbing condition is the implementation of a perfectly matched layer (PML).

The radiation boundary condition is very important in this research because not only that it allows an outgoing wave to leave a domain with no reflection, but it also gives the option of including an incoming wave. Therefore, this condition can also be used to implement a pressure source.

The radiation boundary condition has three wave types available: plane, cylindrical and spherical waves. For a plane wave, this condition is described as

$$\overrightarrow{n} \cdot \left(\frac{1}{\rho_0}(\nabla p - \mathbf{q})\right) + \frac{ikp}{\rho_0} + \frac{i}{2k}\Delta_T p = \frac{i}{2k}\Delta_T p_0 e^{-i(\mathbf{k}\cdot r)} + (ik - i(\mathbf{k}\cdot\overrightarrow{n}))\frac{p_0 e^{-i(\mathbf{k}\cdot r)}}{\rho_0}$$

$$\mathbf{k} = k n_k$$

where p_0 is the pressure source, is ρ_0 is the density, n_k is the wave direction and Δ_T is the Laplace operator in the tangent plane. For a cylindrical wave, the radiation condition is

described by the following equation.

$$\overrightarrow{n} \cdot \left(\frac{1}{\rho_0} (\nabla p - q) \right) = \psi + \frac{r}{2\rho_0(1+ikr)} \Delta_T (p - p_0 e^{-i(\mathbf{k}\cdot r)}) - \left(\frac{i(\mathbf{k} \cdot \overrightarrow{n}) p_0 e^{-i(\mathbf{k}\cdot r)}}{\rho_0} \right) \quad (2.9)$$

where

$$\psi = \left(ik + \frac{1}{2r} - \frac{1}{8r(1+ikr)} \right) \left(\frac{p_0 e^{-i(\mathbf{k}\cdot r)} - p}{\rho_0} \right). \quad (2.10)$$

Lastly, for a spherical wave, the radiation boundary condition is expressed by the following equation.

$$\overrightarrow{n} \cdot \left(\frac{1}{\rho_0} (\nabla p - q) \right) + \left(ik + \frac{1}{r} \right) \frac{p}{\rho_0} - \frac{r \Delta_T p}{2\rho_0(ikr+1)} = \beta \quad (2.11)$$

where

$$\beta = \left(\frac{-r\Delta_T \rho_0}{2\rho_0(ikr+1)} + \left(ik + \frac{1}{r} - iK \cdot \overrightarrow{n} \right) \frac{p_0}{\rho_0} \right) e^{-i\mathbf{k}r}. \quad (2.12)$$

2.4.4 Perfectly Matched Layer

The other absorbing condition is the perfectly matched layer or PML. This condition is often mistaken for a boundary condition when it is actually an extra domain, the digital equivalent of a frequency tuned anechoic chamber, that absorbs the incident waves. Thus, there are no reflections from the exterior boundary when using the PML. However, the PML is only available in the time-harmonic and eigenfrequency analysis in COMSOL Multiphysics. For transient analysis, the radiation boundary is used instead.

CHAPTER 3

OUTDOOR NOISE REDUCTION USING SINUSOIDAL LANDSCAPING

Urban environments are often polluted with low-frequency noise. This type of noise is typically generated by artificial sources including highway traffic, aircraft and industrial machinery. Explosions due to large weapons such as artillery also contribute to the noise pollution. Explosions are particularly hard to deal with since their low-frequency content does not attenuate as quickly as high-frequency noise. Thus, low-frequency noise has the tendency to travel long distances, up to 20 miles in some cases. Additionally, when low-frequency noise interacts with structures such as residential houses, it can cause the structures to rattle or vibrate causing annoyance to the residents.

Low-frequency noise is particularly hard to deal with because of its ability to propagate efficiently and for long distances. A common method of reducing outdoor noise is to put a barrier, typically a wall that contains some type of sound absorbing material, between the source the residential houses. However, this method is only acceptable in places where there is no need for people to cross and is not aesthetically pleasing in general. In places where noise barriers are not welcome, soundproofing the windows and insulating the residential walls are the only options. In 2001, Bradley and Birta [23] made a series of measurements of the sound transmission loss of exterior wood stud walls and determined that the performance of sound insulations of these walls at low frequencies is poor. Since

typical houses contain exterior wood stud walls, the loudest noise the residents inside the houses will experience are low-frequencies noise. Thus, in order to achieve better overall sound reduction, it is very important to focus on suppressing the low-frequency noise.

Most theoretical and experimental work on outdoor noise reduction involved barriers and insulations [18-23]. When these methods are ineffective against low-frequency noise, then different anti-propagation methods must be taken into consideration.

We consider using undulating landscaping, e.g., a sinusoidally shaped boundary condition as a method to suppress low-frequency outdoor noise. While such a method can be expensive, it is aesthetically appealing and does not preclude other uses of the land. Undulating boundary conditions have been proposed and used in microwave communications where waveguides have corrugated surfaces. Our work is largely motivated by this work, and we will use the terms "undulating landscaping", "undulating boundary conditions" and "corrugation" interchangeably. The problem involving acoustic waves interfacing with a corrugated surface has been extensively studied over the past century.

The theoretical analysis of this problem was first conducted by Lord Raleigh [24]. Feshbach and Clogston examined and generalized the perturbation method of solving boundary value problems with irregular boundary conditions [25]. Various investigators have conductor studies involving corrugated surfaces [26-31]. Asfar analytically and numerically investigated the TE_{10} mode in a rectangular corrugated waveguide that had a phase shift halfway into the corrugation [32]. Asfar's investigation showed that there is a narrow passband among a wider stopband. Therefore, it is possible for corrugated waveguide can act as a stopband filter. This is important because we want to stop the low-frequency

acoustic waves from propagating. Boulanger et al. measured the relative sound pressure level over hard surfaces containing random or periodically spaced roughness [33]. They found that additional diffraction grating effects and greater relative SPL minima can be achieved by having periodic roughness on a hard surface. Other investigations involving rough surfaces were conducted by Potel et al. [34] and Fawcett [35].

3.1 Theoretical Background

The propagation of waves can be described by the wave equation.

$$\nabla^2 p = \frac{1}{c^2}\frac{\partial^2 p}{\partial t^2} \tag{3.1}$$

Using separation of variables, Equation (3.1) can be simplified into time-independent equation

$$\nabla^2 P + k^2 P = 0 \tag{3.2}$$

where

$$k = \frac{\omega}{c}. \tag{3.3}$$

In Equation (3.2), k is the wavenumber, ω is angular frequency, c is the speed of sound, and P is a spatial function defined on three-dimensional Euclidean space.

The geometry of the corrugated surface is shown in Figure 3.1 and described by

$$f(x) = A\sin(\frac{2\pi x}{d} + \theta) \tag{3.4}$$

where A is the amplitude, d is the wavelength and θ is the phase. In Figure 3.1, 'PT1' is the point source, 'a' is the length of the corrugation, 'b' is the period and 'c' is the amplitude.

Equation (3.4) can be modified for the case in which the wavelength of the undulating boundary condition is continuously decreasing. This is shown in Equation (3.5).

$$f(x) = A\sin\left[(k_0 + ax)x\right] \tag{3.5}$$

where

$$a = \frac{(k_f - k_0)}{D},$$

k_0 is the initial wavenumber, k_f is the final wavenumber, D is the total corrugation length or distance and x is the distance along the propagation direction.

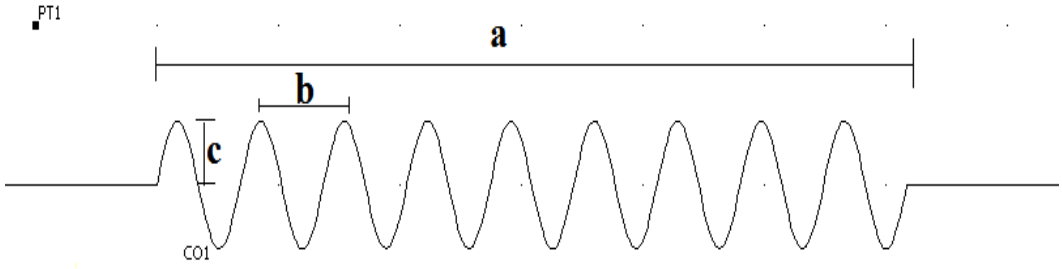

Figure 3.1. Corrugated surface

The speed of sound traveling through the ground is given by

$$c_g = \sqrt{\frac{E}{\rho}} \tag{3.6}$$

where E is Young's modulus and ρ is the density of the ground.

A sound wave propagating outdoor over a flat surface will always lose energy as it propagates. We, therefore, are interested in how much additionally loss can occur if the surface is corrugated. This additional loss is calculated using

$$L = SPL_f - SPL_c \tag{3.7}$$

where L is the loss (dB), SPL_f is the sound pressure level obtained from the model with a flat granite surface and SPL_c is the sound pressure level obtained from the models with a corrugated granite surface.

3.2 Finite element Model Setup

The finite element model is 110 meters long and 50 meters in height including the perfectly matched layers (PML) each having a width of 5 meters. The model geometry is shown in Figure 3.2. Regions R1 through R8 are the perfectly matched layers. The region, C02, is consisted of air with a density of $1.25\ kg/m^3$. The ground (region C01) is made of granite having a density of $2600\ kg/m^3$. The reason for choosing granite is that it provide a hard surface for the acoustic wave to interface with. In practice, the ground is soft and absorbs acoustic energy more efficiently. The acoustic point source with a power of 100 Watts is located at point PTL which is 5 meters above the ground.

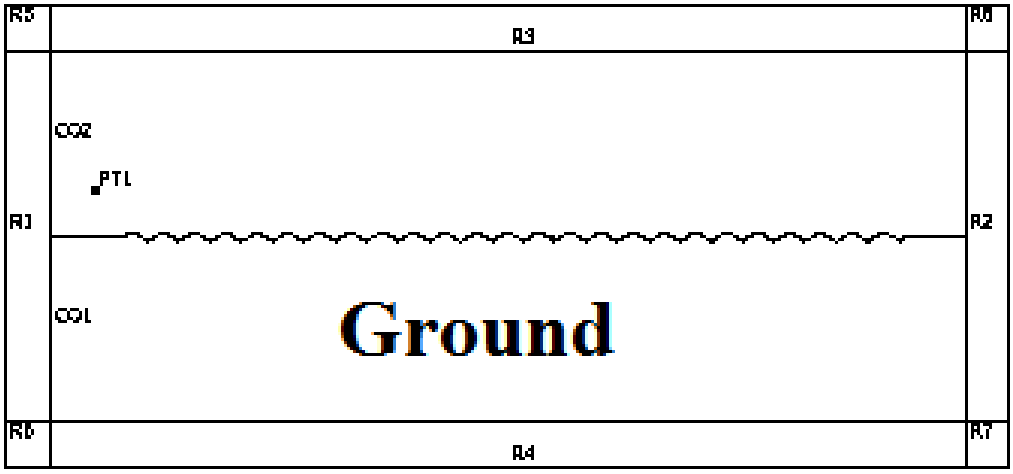

Figure 3.2. The geometry of the finite element model

Other properties are listed in the Table 3.1. The point of measurement is 90 meters away from the source and 5 meters above the ground. The amplitude, length and phase of the corrugation are changed from one model to another to see what affect these parameters have on the loss. These changes are discussed in greater details in the following sections.

Table 3.1. Parameters used in the finite element simulation

Parameter	Value	Description
c_s	$343[m/s]$	Speed of sound in air
c_g	$4803.84[m/s]$	Speed of sound in granite
ρ_a	$1.25[kg/m^{3]}$	Density of air
ρ_g	$2600[kg/m^3]$	Density of granite
p_o	$100[W]$	Source power

Time-harmonic simulations are run from 5Hz to 150Hz. The maximum element size is chosen to be small enough so that reasonable solutions can be obtained, but at the same time does not cause the computer to run out of memory. The result from a simulation of a model with perfectly flat ground surface is used as a baseline and to calculate the loss due to having a corrugated surface using Equation (3.7).

3.3 Corrugation with Different Lengths

In order to study the effect of different corrugation lengths on the loss, the corrugation length is varied from 10.28 meters to 51.45 m at 10.28 m intervals. The wavelength and amplitude of the corrugation are kept constant at 3.43 m and 2 m respectively. We choose to increment the corrugation length by 10.28 m or three wavelengths at time rather than 3.43 m or one wavelength. The reason for this is that a single wavelength of the corrugation acts similar to small barrier.

3.4 Corrugation with Different Amplitudes

The amplitude of the corrugation is varied from 0.2 m to 2 m at 0.2 m intervals. This is increment interval is small enough for the effect of the amplitude on the transmission loss to be observed, yet large enough to affect the propagation of the acoustic wave. The corrugation wavelength is held constant at 3.43 m. The length of the corrugation remains 85.75 m while the amplitude is varied. Again, the point source location is located at 5 m above the granite and 3 m before the starting point of the corrugation.

3.5 Corrugation with Continuously Decreasing Wavelength

To study the effect of a decreasing corrugation wavelength on the transmission loss, we created a finite element model containing a surface corrugation described by Equation (3.5). The geometry is shown in Figure 3.3. The initial wavelength is set 15 m. Thus, k_0 is 0.4189 m^{-1}. The final wavelength is 2 m and k_f is π. The corrugation length, D, is chosen to be 74 m which is long enough to observe the effect of this corrugation on the transmission loss. The amplitude is chosen to be constant at 2 m. The source and measurement locations are same as previously mentioned.

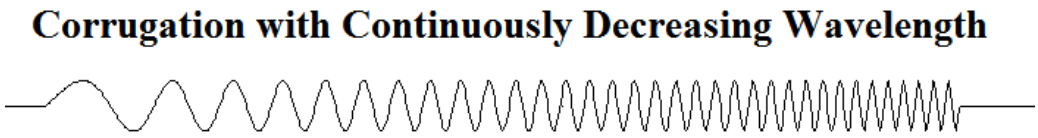

Figure 3.3. The geometry of the surface with a continuously decreasing wavelength

3.6 Corrugation with Phase Shifts

Asfar examined the stopband filter characteristics of boundary periodic corrugation in a waveguide [32]. He used a rectangular waveguide containing a phase shift half way into the corrugation and showed that a narrow passband filter can be formed. We consider applying phase shift to our corrugation to see what effects it will have in an outdoor environment. Two simulations are performed to study the transmission loss if there is a phase change in the corrugation. The first model contains a surface with a corrugation length of 61.74 meters and a constant phase of zero degrees. The second model has a phase shift of 180 degrees half way into the corrugation. The corrugation length of the second model is the same as the first model. Figure 3.4 shows the geometry of the corrugation containing phase shifts. The amplitude of the corrugation of both models are two meters. The results are these two simulations are compared with the result obtained from a simulation whose model contains no phase shift.

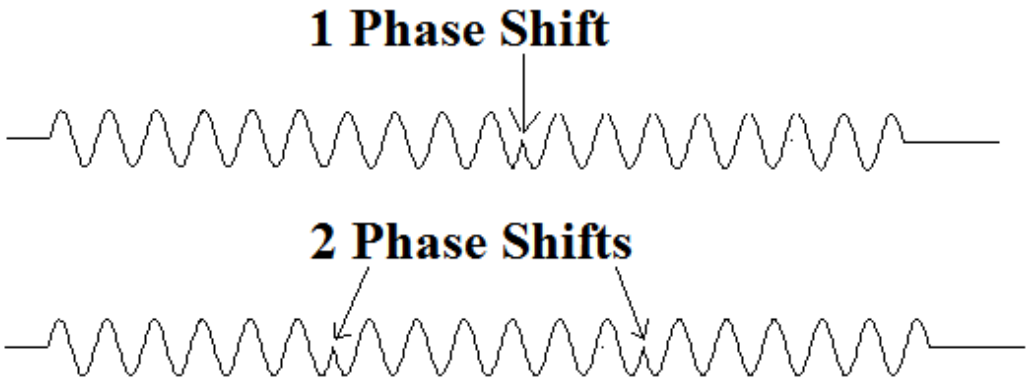

Figure 3.4. Corrugation containing 180 degrees phase shifts

3.7 Results

Contour plots of the sound pressure level of the model containing a smooth surface are shown in Figures 3.5 and 3.6 for two sound frequencies, 50 and 100Hz. Figures 3.7 and 3.8 are the contour plots of the sound pressure level of the model containing a corrugated surface with a corrugation amplitude of 1 m, corrugation wavelength of 3.43 m and corrugation length of 85.75 m. The effect of the corrugation length on the transmission loss is shown in Figure 3.9.

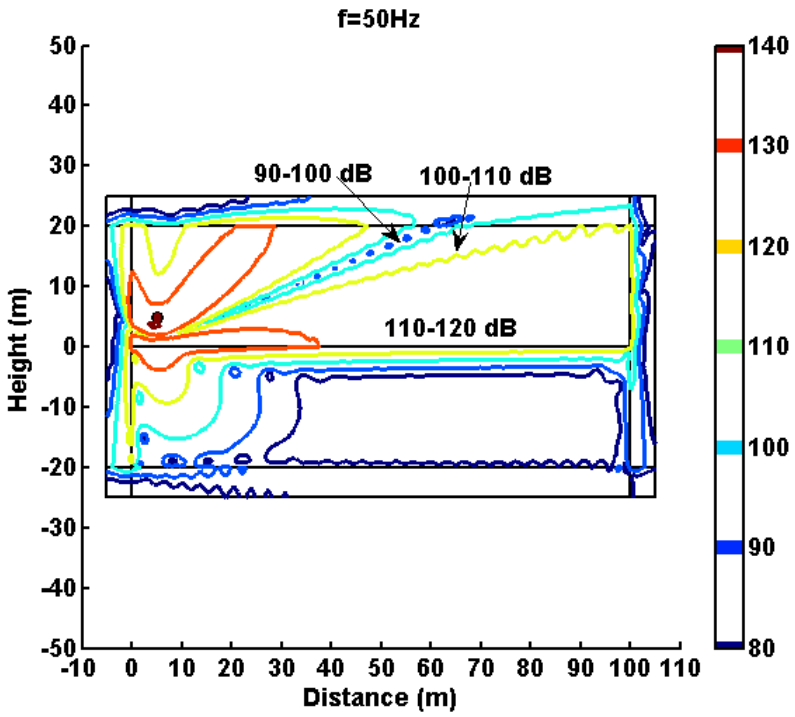

Figure 3.5. Contour plot of the SPL (dB) for a smooth surface at 50 Hz

The results show that increasing the length of the corrugation shifts the loss spectrum upward resulting in higher loss. For a corrugation length of 10.29 m, the maximum loss is 11.03 dB which occurs at 25 Hz, and the minimum loss is -1.1 dB which occurs at

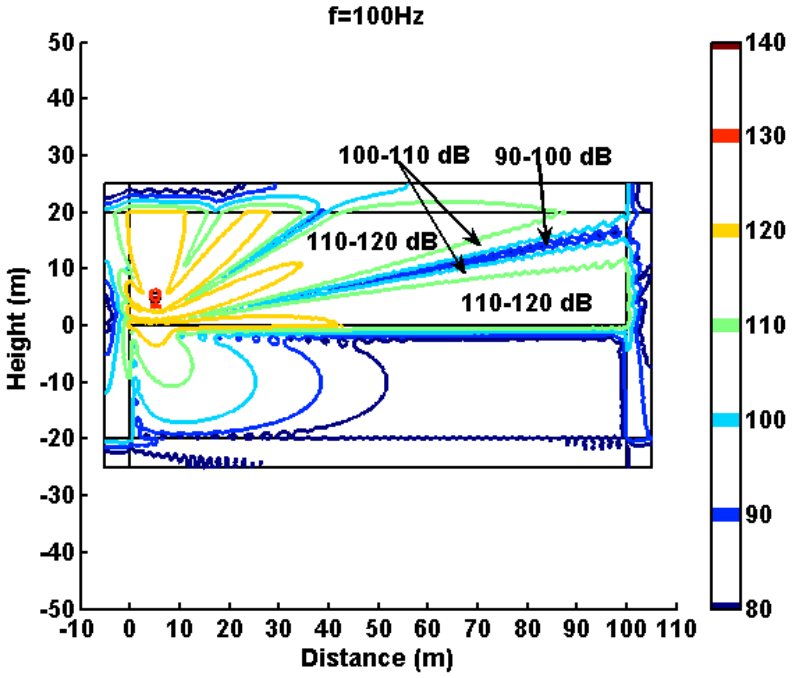

Figure 3.6. Contour plot of the SPL (dB) for a smooth surface at 100 Hz

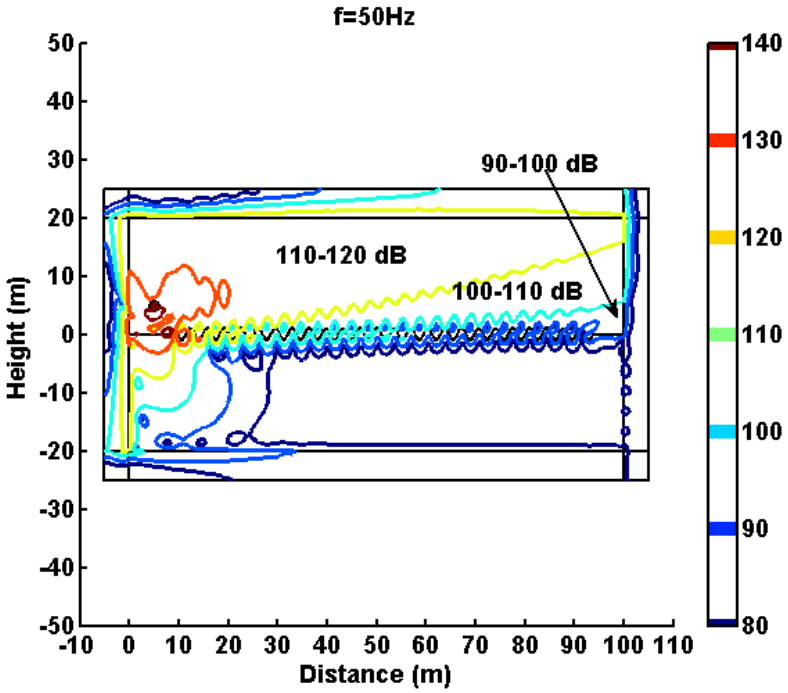

Figure 3.7. Contour plot of the SPL (dB) for a corrugated surface at 50 Hz

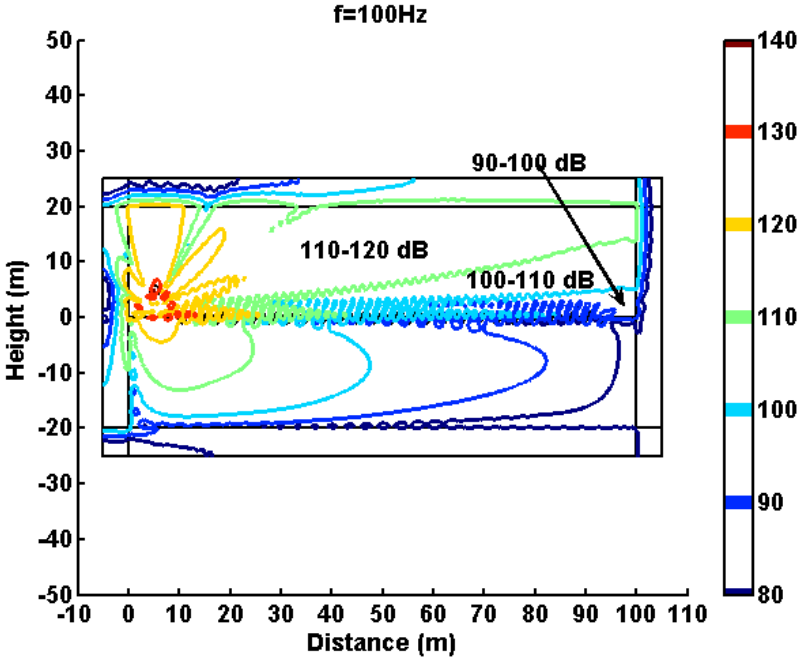

Figure 3.8. Contour plot of the SPL (dB) for a corrugated surface at 100 Hz

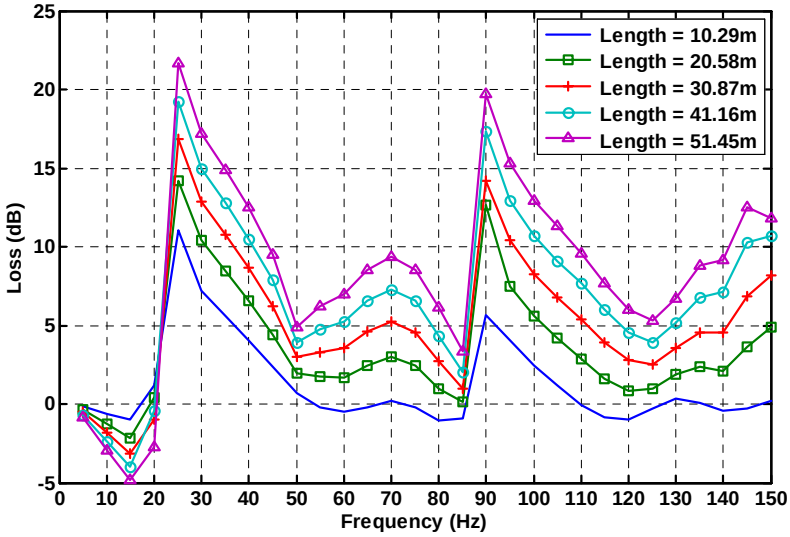

Figure 3.9. Loss due to different corrugation lengths

80 Hz. When the corrugation length is incremented by 10.29 m, the maximum loss remains at 25 Hz, but it is increased to 14.21 dB from 11.03 dB. Our results indicate that there is a shift in the highest peak by an average of 3.2 dB for each increment of 10.29 m. Table 3.2 shows length of the corrugation, the maximum loss, and the minimum loss where L_x is the maximum loss and f_x (Hz) indicates the frequency in which the maximum loss occurs, and L_n is the minimum loss and f_n (Hz) indicates the frequency at which the minimum loss occurs.

Table 3.2. Maximum and minimum loss

Length(m)	L_x(dB)	f_x(Hz)	L_n(dB)	f_n(Hz)
10.29	11.03	25	-1.1	80
20.58	14.21	25	-2.14	15
30.87	16.85	25	-3.12	15
41.16	19.2	25	-3.98	15
51.45	21.7	25	-4.8	15
61.74	24.5	25	-5.68	15
72.03	28.28	25	-6.59	15
82.32	33.42	25	-7.24	15

When the length of the corrugation is held constant at 85.75 m and the amplitude is varied, the first peak (maximum loss) in Figure 3.10 shifts to the left as the amplitude of the corrugation is increased. The simulation results, therefore, indicate that increasing the amplitude of the corrugation will shift the first resonance frequency to a lower frequency. For a corrugation amplitude of 0.2 m, the first peak in Figure 3.10 with a value of 6.81 dB appears at 50 Hz. When the amplitude is increased to 0.4 m, not only that the peak increases drastically to 33.7 dB, it also shifted by 2 Hz. On average, the first resonance frequency shifts to the left by 3.2 Hz for a 0.2 m increase in the corrugation amplitude.

The effect of a corrugation with a continuously decreasing wavelength on the transmission loss is shown in Figure 3.11. The result of a simulation of a model containing

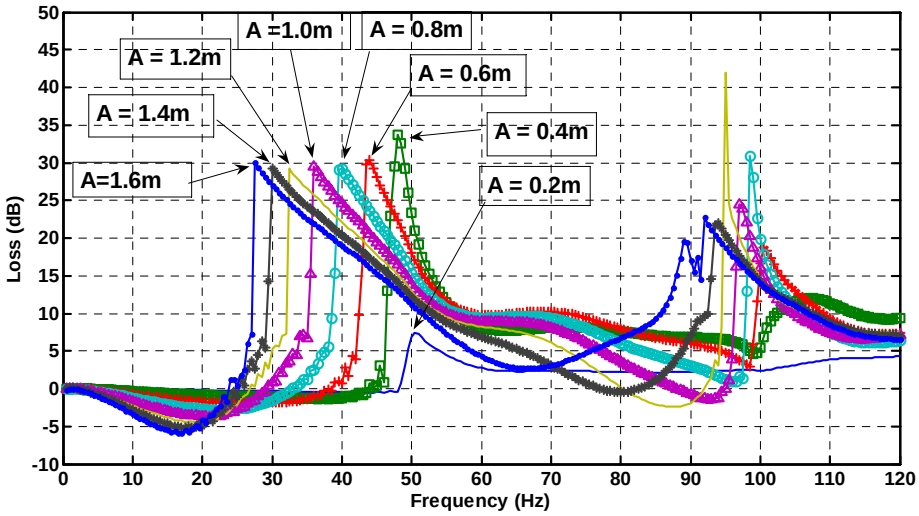

Figure 3.10. The effect of the corrugation amplitude on the transmission loss

a constant wavelength of 3.43 m and amplitude of 2 m is also plotted in the same graph for comparison. Note that the corrugation with the constant wavelength is longer than the one with a decreasing wavelength by 11 m. As previously discussed, this will cause the corrugation with a constant wavelength to have a slightly higher loss at the first resonance frequency.

The results of the two models, one containing a single phase shift of 180 degrees half wave into the corrugation and the other containing two phase shifts of 180 degrees are compared with a model containing no phase shift. Figure 3.12 shows the effect of the phase shift in the corrugation on the transmission loss. One can see that changing the phase of the corrugation has no major effect on the transmission loss in an outdoor environment.

We used finite element simulations to show that an undulating boundary conditions (undulating landscaping) can be used as an effective anti-propagation method to reduce

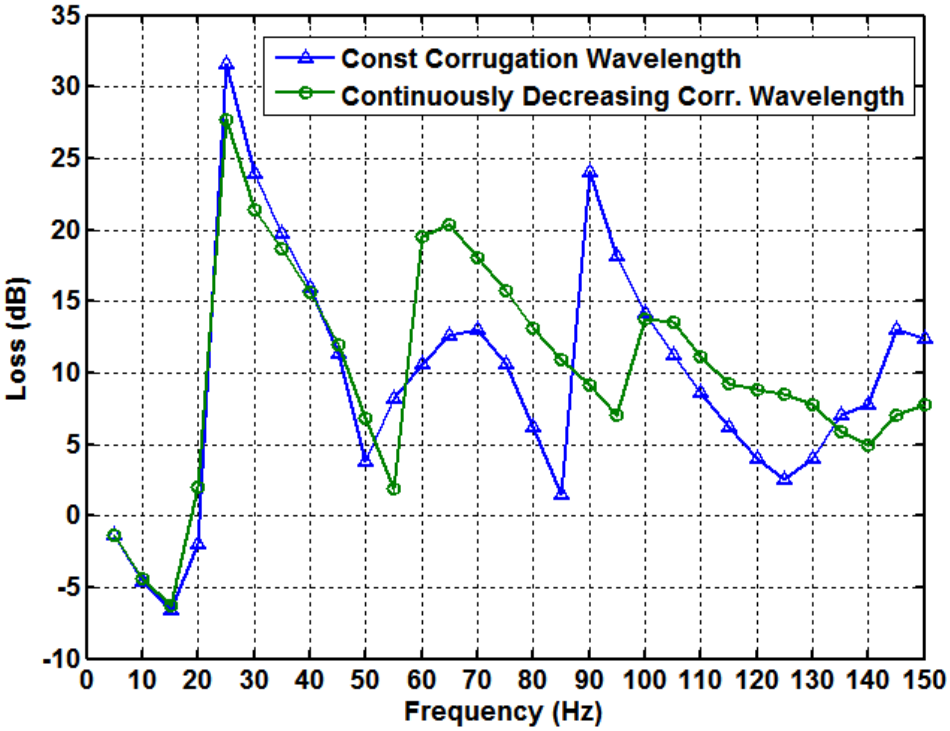

Figure 3.11. Transmission loss due to a decreasing wavelength

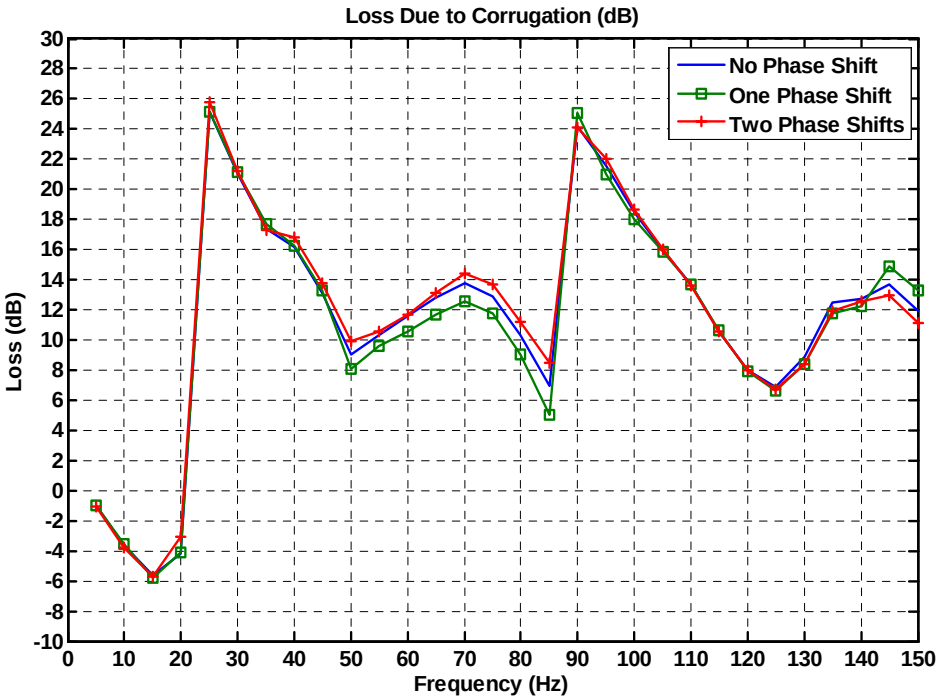

Figure 3.12. The effect of phase shift in the corrugation on the transmission loss

low-frequency outdoor noise. For a corrugation with a wavelength of 3.43 m, amplitude of 2 m and a corrugation length of 82.32 m, the first resonance occurs at 25 Hz. At this frequency, the additional loss due to the undulating boundary is 33.42dB. We also showed that the undulating landscape create a significant shielding effect at low frequency and close to the ground beyond the landscaping. We show that increasing the corrugation length increases the loss. Changing the amplitude of the corrugation while keeping the length and wavelength of the corrugation constant cause the first resonance frequency to shift. Finally, having phase shifts in the corrugation does not significantly affect the transmission loss in an outdoor environment.

CHAPTER 4

SURFACE MODELING USING EQUIVALENT SOURCES

Even though there is significant progress in modeling acoustic fields using finite element and boundary element methods, there are still shortcomings that these two methods have to overcome. These shortcomings were discussed by Koopmann et al. [36-37]. It includes the difficulty of approximating the Helmholtz integral in numerical form, uniqueness problem and singularity of the Green function and complexity which leads to an increase in computations. These drawbacks motivated researchers to find a more straightforward and simpler computational method. In their research, Koopmann et al. investigated the method of using the principle of wave superposition to compute acoustic fields. The superposition method, an idea that stemmed from the calibration procedure used in boundary-element studies, offers several advantages over the boundary-element method. These advantages include decrease in computations due to the lack of uniqueness and singularities and simple generation of the matrix elements due to having nodes as the basis for the formulation, not elements as in the boundary-element method. Additionally, the superposition method offers improved accuracy over the boundary-element method for a similar density of nodes.

The superposition method also called equivalent source method (ESM) is based on the concept that an acoustic field generated by a radiator can be estimated using an array of simple acoustic sources placed inside of the radiator. The accuracy of the estimated field depends on the locations, complex amplitudes and density of the simple sources. In

1992, the robustness and stability of the superposition method was investigated by Jeans and Mathews [38]. The robustness of the superposition method can be improved by using a hybrid of monopole and dipole sources to overcome the problem of nonuniqueness at certain frequencies. It should be mentioned that although earlier researchers referred to this method as the superposition method, the term equivalent source method is widely used and therefore, is used in the succeeding chapters.

Johnson et al. [39] used the equivalent source method to compute the internal pressure field of a radiator. In their investigation, a rectangular with rigid wall is used as the enclosure. The approximation of the behavior of the boundary is determined by the strength of the equivalent sources. This means that the source strengths must be calculated before the pressure field can be approximated. A matrix formulation can be used to find the equivalent source strengths. Detailed methods to find the source strengths are discussed by Nelson and Yoon [40, 41]. Pinho and Arruda compared the equivalent source method with NAH and concluded that good acoustic source reconstruction can be obtained using the ESM [42]. Bouchet *et al*. used an equivalent sphere rather than a distribution of equivalent sources where each point on the structure corresponds to a point on the sphere [43]. The ESM has been used by some researchers to study sound propagation through urban street canyon [44]. In this dissertation, ESM is applied to study waves propagating over corrugated surfaces.

4.1 Green's Function

A pressure field generated by a point source can be described by the inhomogeneous Helmholtz equation,

$$\nabla^2 G(R) + k^2 G(R) = \delta(x - x_0) \tag{4.1}$$

where R is the direct distance from the source to a field point and δ is a Dirac delta function. The solution to Equation (4.1) is the free field Green's function which is represented by G and is used to compute the pressure field [39]. For three dimensional problems, the free field Green's function is expressed mathematically as

$$G(R) = \frac{e^{ikR}}{4\pi R} \tag{4.2}$$

where R is Euclidean norm and given as

$$R = \|[(x - x_0), (y - y_0)]\| \tag{4.3}$$

where (x_0, y_0) is the location of the source.

4.2 Single Source in Free Space

Consider a single acoustic source in free space, the total complex amplitude of pressure which emanates from that point source is given as

$$\phi(R) = \frac{Ae^{ikR}}{4\pi R} \tag{4.4}$$

where R is the distance from the source to the point of interest and k is the wavenumber. Notice that Equation (4.4) is the same as Equation (4.2) with a source strength A. Its

derivative with respect to x is

$$\begin{aligned}\frac{\partial\phi}{\partial x} &= -\frac{Ae^{ikR}}{4\pi R^2}\frac{\partial R}{\partial x} + \frac{Ae^{ikR}}{4\pi R}ik\frac{\partial R}{\partial x} \\ &= \frac{Ae^{ikR}}{4\pi R}\left(-\frac{1}{R} + ik\right)\frac{\partial R}{\partial x}\end{aligned}$$

Usually if R is between the test point and the source point (x_0, y_0) then

$$\frac{\partial R}{\partial x} = \frac{(x - x_0)}{R}$$

In short

$$\frac{\partial\phi}{\partial x} = \frac{Ae^{ikR}}{4\pi R}\left(-\frac{1}{R} + ik\right)\frac{(x - x_0)}{R}$$

and hence

$$\frac{\partial\phi}{\partial x} = \frac{Ae^{ikR}(x - x_0)}{4\pi R}\left(-\frac{1}{R^2} + \frac{ik}{R}\right) \tag{4.5}$$

$$\frac{\partial\phi}{\partial y} = \frac{Ae^{ikR}(y - y_0)}{4\pi R}\left(-\frac{1}{R^2} + \frac{ik}{R}\right) \tag{4.6}$$

Equations (4.5) and (4.6) express the potential velocity and are important for calculating the conditions at the boundary.

4.3 Multiple Sources in Free Space

If there is pressure emanating from multiple sources located at (x_j, y_j) and the pressure of the sources is given in Equation (4.4), then

$$\frac{\partial\phi}{\partial x} = \sum_j \left(\frac{ikA_j e^{ikR_j}}{4\pi R_j^2} - \frac{A_j e^{ikR_j}}{4\pi R_j^3}\right)x + \sum_j \left(\frac{A_j e^{ikR_j}}{4\pi R_j^3} - \frac{ikA_j e^{ikR_j}}{4\pi R_j^2}\right)x_j \tag{4.7}$$

$$\frac{\partial \phi}{\partial y} = \sum_j \left(\frac{ikA_j e^{ikR_j}}{4\pi R_j^2} - \frac{A_j e^{ikR_j}}{4\pi R_j^3} \right) y + \sum_j \left(\frac{A_j e^{ikR_j}}{4\pi R_j^3} - \frac{ikA_j e^{ikR_j}}{4\pi R_j^2} \right) y_j \tag{4.8}$$

where R_j is the direct distance from source (x_j, y_j). Equations (4.7) and (4.8) are derived as follows.

Let ϕ_j represent the complex amplitude emanating from the jth source. Then $\phi = \sum_j \phi_j$. Then

$$\frac{\partial \phi_j}{\partial x} = \sum_k \frac{\partial \phi_j}{\partial R_k} \frac{\partial R_k}{\partial x} = \frac{\partial \phi_j}{\partial R_j} \frac{\partial R_j}{\partial x}$$

because ϕ_j depends on R_j only. The pressure of a single source is given in Equation (4.4).

$$\frac{\partial \phi_j}{\partial R_j} = \frac{ikA_j e^{ikR_j} (4\pi R_j)}{(4\pi R_j)^2} - \frac{4\pi A_j e^{ikR_j}}{(4\pi R_j)^2} \tag{4.9}$$

Hence, collecting all terms leads to

$$\frac{\partial \phi}{\partial x} = \sum_j \left(\frac{ikA_j e^{ikR_j}}{4\pi R_j} - \frac{A_j e^{ikR_j}}{4\pi R_j^2} \right) \frac{(x - x_j)}{R_j} \tag{4.10}$$

$$= \sum_j \left(\frac{ikA_j e^{ikR_j}}{4\pi R_j^2} - \frac{A_j e^{ikR_j}}{4\pi R_j^3} \right) (x - x_j) \tag{4.11}$$

$$= \sum_j \left(\frac{ikA_j e^{ikR_j}}{4\pi R_j^2} - \frac{A_j e^{ikR_j}}{4\pi R_j^3} \right) x + \sum_j \left(\frac{A_j e^{ikR_j}}{4\pi R_j^3} - \frac{ikA_j e^{ikR_j}}{4\pi R_j^2} \right) x_j \tag{4.12}$$

We can derive $\frac{\partial \phi}{\partial y}$ for a multi-source system the same way. Equations (4.7) and (4.8) are important in computing the boundary conditions where more than one source are involved.

4.4 Outdoor Propagation Over a Hard Surface

When acoustic waves propagate outdoor, there are two main boundary conditions to consider. There is the ground or surface below which specifies the first condition. The waves are not bounded above which is the second condition. The sound pressure propagat-

ing above a hard ground is the solution to the following system given by Filippi et al. [45] and based on Helmholtz equation

$$\nabla^2\phi(r) + k^2\phi(r) = f(r) \tag{4.13}$$

$$\frac{\partial\phi(r)}{\partial\overrightarrow{n}} + \frac{ik}{\varsigma}\phi(r) = 0 \tag{4.14}$$

$$\lim_{r\to\infty}\phi = O\left(r^{(1-n)/2}\right) \tag{4.15}$$

$$\lim_{r\to\infty}(\partial_r\phi - ik\phi) = o\left(r^{(1-n)/2}\right) \tag{4.16}$$

where $f(r)$ is the source function, r is the distance from the source, ϕ and k are the complex pressure and wavenumber respectively, ς is the ratio of the ground impedance to the impedance of the air and n is the dimension of space. The case $n = 2$ represents an infinite line source and $n = 3$ represents a point source. Equations (4.15) and (4.16) define the Sommerfield radiation conditions. Equation (4.14) is the ground surface boundary condition. If the surface of the ground is assumed to be hard with infinite impedance, then ς is infinite as well, and Equation (4.14) becomes

$$\nabla\phi\cdot\overrightarrow{n} = 0 \tag{4.17}$$

where $\vec{n}$ is a unit vector that is orthogonal to the hard boundary. If the hard boundary (ground) is completely flat and horizontal then $\overrightarrow{n}$ is in the y-direction, and it is constant. The equation above can be reduced to

$$\frac{\partial\phi}{\partial y} = 0, \text{ for } \overrightarrow{n} = \begin{bmatrix} 0 \\ 1 \end{bmatrix}. \tag{4.18}$$

For a hard flat surface, the solution to Equations (4.13)-(4.16) is of the form

$$\phi = \frac{Ae^{ikR_1}}{4\pi R_1} + \frac{Ae^{ikR_2}}{4\pi R_2} \tag{4.19}$$

where R_1 is the distance from the Source 1 to the point of interest, R_2 is the distance from the Source 2 (the image) to the point of interest, A is the complex amplitude and k is the wavenumber. Equation (4.19) is independent of time, but the time-harmonic term, $e^{j\omega t}$ easily can be recovered.

4.5 Modeling Hard Surface Using Acoustic Sources

A $2-$D surface may be defined on the $x-y$ plane by placing acoustic sources on that plane. Consider a case where the hard surface of the ground is completely flat, to define this flat surface, we can place two sources with the same frequency and strength on the x-y plane. The surface, then, lies midway between the two sources as shown in Figure 4.1. The actual physical source is source 1 with source 2 being its image. In order to model a more complex surface such as an undulating surface, we have to use more than two sources. To do this, we let source 1 remain as the actual physical source and source 2 as its image. Smaller acoustic sources are placed at various locations along the x-axis which will cause the flat surface to deform. The shape and degree of deformation of the flat surface is determined by the amplitudes of the small sources as shown in Figure 4.2.

4.5.1 Theoretical Derivation

If the ground is undulated, the normal vector $\overrightarrow{n}$ in Equation (4.17) is no longer constant, but varies as the geometry of the ground varies. To form an undulating surface,

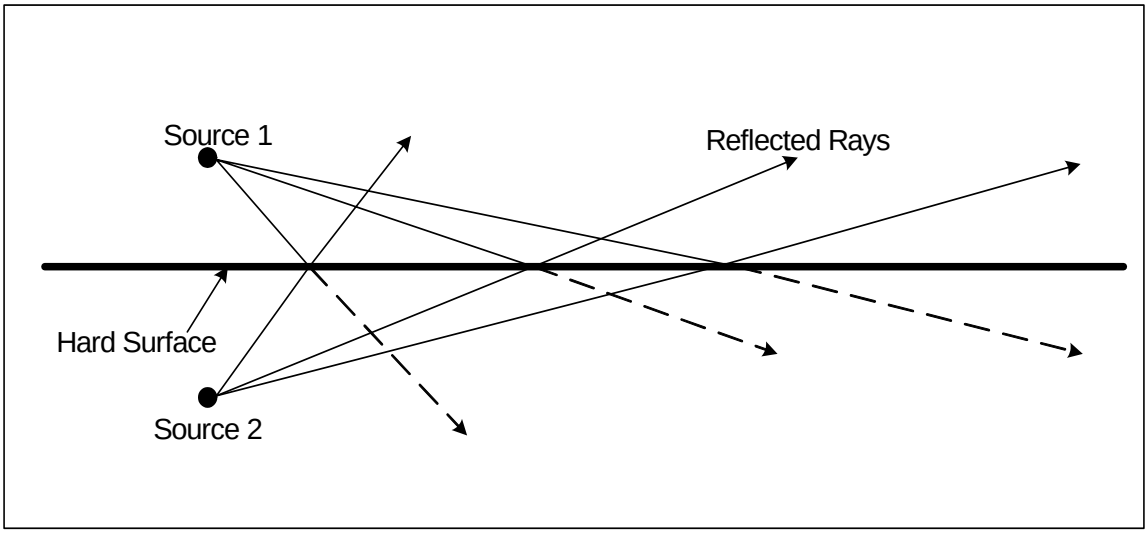

Figure 4.1. A flat hard surface is modeled by placing two sources of equal strength

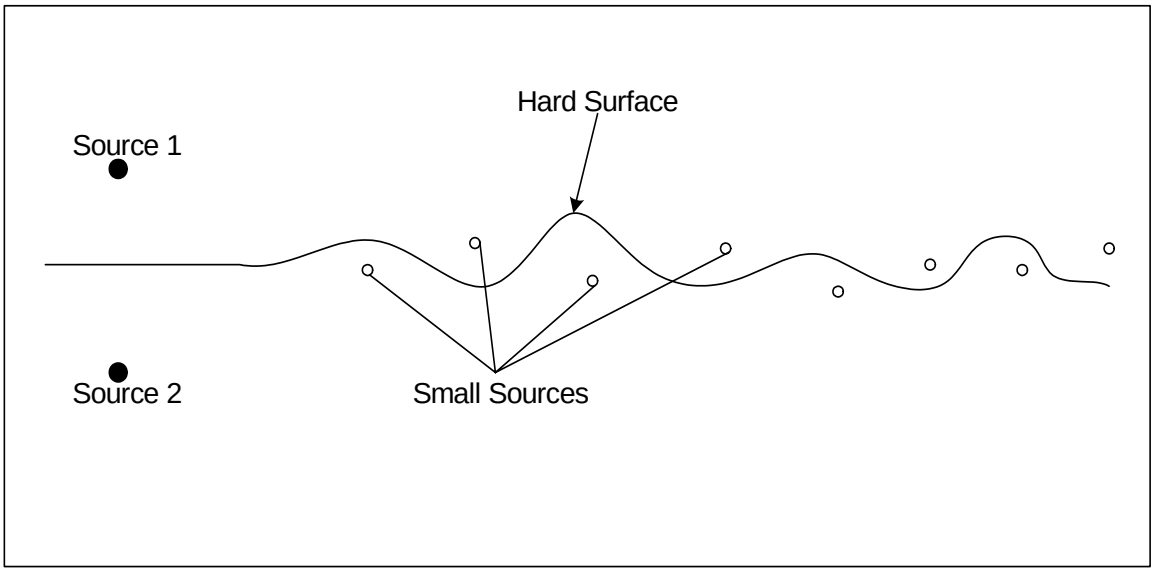

Figure 4.2. Different surface shapes can be formed using small acoustic sources

the two sources depicted in

$$\phi = \sum_{i}^{n} \frac{A_1 e^{ikR_i}}{4\pi R_i}, \tag{4.20}$$

where n is the total number of sources. Here, A_i is the complex amplitude of source i.

$$A_1 = A_2 = O\left(1\right), \tag{4.21}$$

and

$$|A_i| = O\left(\frac{\epsilon}{R_i}\right), \tag{4.22}$$

where ϵ is a small number and R_i is the distance of Source i to the main source. In general, since ϕ is complex, and its derivatives are also complex

$$\frac{\partial \phi}{\partial x} = \mathrm{Re}\left(\frac{\partial \phi}{\partial x}\right) + \mathbf{j}\,\mathrm{Im}\left(\frac{\partial \phi}{\partial x}\right), \tag{4.23}$$

$$\frac{\partial \phi}{\partial y} = \mathrm{Re}\left(\frac{\partial \phi}{\partial y}\right) + \mathbf{j}\,\mathrm{Im}\left(\frac{\partial \phi}{\partial y}\right), \tag{4.24}$$

and representing $\vec{n}$ as $n = [n_1, n_2]^{\mathsf{T}} \in \mathbb{R}^2$, Equation (4.17) becomes

$$\begin{aligned} 0 &= n^{\mathsf{T}} \nabla \phi = n_1 \frac{\partial \phi}{\partial x} + n_2 \frac{\partial \phi}{\partial y} \\ &= n_1\,\mathrm{Re}\left(\frac{\partial \phi}{\partial x}\right) + n_2\,\mathrm{Re}\left(\frac{\partial \phi}{\partial y}\right) + \\ &\quad \mathbf{j}\left[n_1\,\mathrm{Im}\left(\frac{\partial \phi}{\partial x}\right) + n_2\,\mathrm{Im}\left(\frac{\partial \phi}{\partial y}\right)\right]. \end{aligned} \tag{4.25}$$

Both the real part and imaginary parts must vanish:

$$n^{\mathsf{T}} \begin{bmatrix} \mathrm{Re}\left(\frac{\partial \phi}{\partial x}\right) & \mathrm{Im}\left(\frac{\partial \phi}{\partial x}\right) \\ \mathrm{Re}\left(\frac{\partial \phi}{\partial y}\right) & \mathrm{Im}\left(\frac{\partial \phi}{\partial y}\right) \end{bmatrix} = 0, \tag{4.26}$$

which can only happen if the matrix is singular, or:

$$0 = d(x,y) = \det \begin{bmatrix} \mathrm{Re}\left(\frac{\partial\phi}{\partial x}\right) & \mathrm{Im}\left(\frac{\partial\phi}{\partial x}\right) \\ \mathrm{Re}\left(\frac{\partial\phi}{\partial y}\right) & \mathrm{Im}\left(\frac{\partial\phi}{\partial y}\right) \end{bmatrix} \tag{4.27}$$

$$\begin{aligned} = \; & \mathrm{Re}\left(\frac{\partial\phi}{\partial x}\right)\mathrm{Im}\left(\frac{\partial\phi}{\partial y}\right) - \\ & \mathrm{Im}\left(\frac{\partial\phi}{\partial x}\right)\mathrm{Re}\left(\frac{\partial\phi}{\partial y}\right). \end{aligned} \tag{4.28}$$

This is a condition that is independent of $\vec{n}$. Once x and y are found such that the determinant above is zero, then n can be found as a null vector of the shown matrix.

4.5.2 Conditions For a Hard Surface

In order for a contour to be a hard surface, Equation (4.17) must be satisfied. It is difficult to find locations on the plane where this equation is satisfied without knowing the normal vector, $\vec{n}$. Therefore, other conditions must be established if we wish to obtain the locations of the surface at every point on the x-axis. We have already established one condition in the previous section. We determined that on the hard surface Equation (4.28) must equal zero. Now we look at the cross product as shown below where a is a vector comprised of the real part of $\frac{\partial\phi}{\partial x}$ and $\frac{\partial\phi}{\partial y}$, and b is a vector comprised of the imaginary part of $\frac{\partial\phi}{\partial x}$ and $\frac{\partial\phi}{\partial y}$.

$$a = \left[\mathrm{Re}\left(\frac{\partial\phi}{\partial x}\right), \mathrm{Re}\left(\frac{\partial\phi}{\partial y}\right), 0\right] \tag{4.29}$$

$$b = \left[\mathrm{Im}\left(\frac{\partial\phi}{\partial x}\right), \mathrm{Im}\left(\frac{\partial\phi}{\partial y}\right), 0\right] \tag{4.30}$$

The cross product is given as

$$z = a \times b \tag{4.31}$$

where

$$z = [i, j, k] \tag{4.32}$$

We can assume that at any point on the surface, the real and the imaginary components of the gradient are parallel. In another words, on the surface, the components of z are zero if the angle between a and b is 180 or 0 degree. For visualization, refer to Figure 4.3.

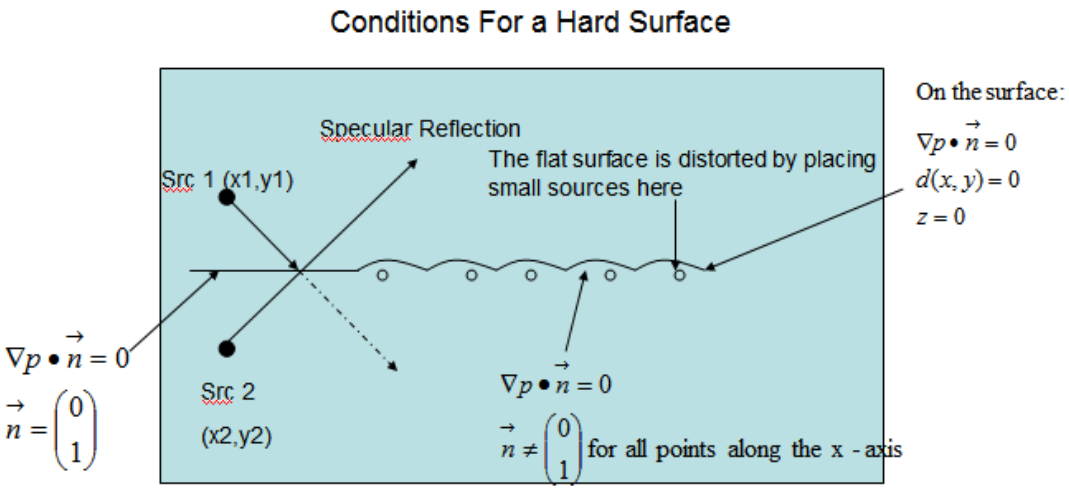

Figure 4.3. Conditions for a hard surface

4.5.3 Finding the Surface

When placing small acoustic sources with various amplitudes spread out at certain interval along the x-axis, it is not obvious where the surface lies. This is shown in Figure 4.4. The total pressure, p, is the summation of the pressure emanating from all the sources, $\phi(R_1)$ to $\phi(R_n)$. The expression for $\phi(R_n)$ is given by Equation (4.4) where R_n is the

direct distance from source n to the point of interest. The top plot is a plot of the sound pressure level of only the main source and its image. It is clear that the hard surface lies halfway between the two sources for all points on the x-axis. The bottom plot contains the main source and its image in addition to three additional sources. It is difficult to know the location of the surface near the small sources since there are distortions on the surface. Therefore, to locate the surface at all points along the x-axis, we use an algorithm to check for the locations where the conditions defined in section 4.5.2 are satisfied.

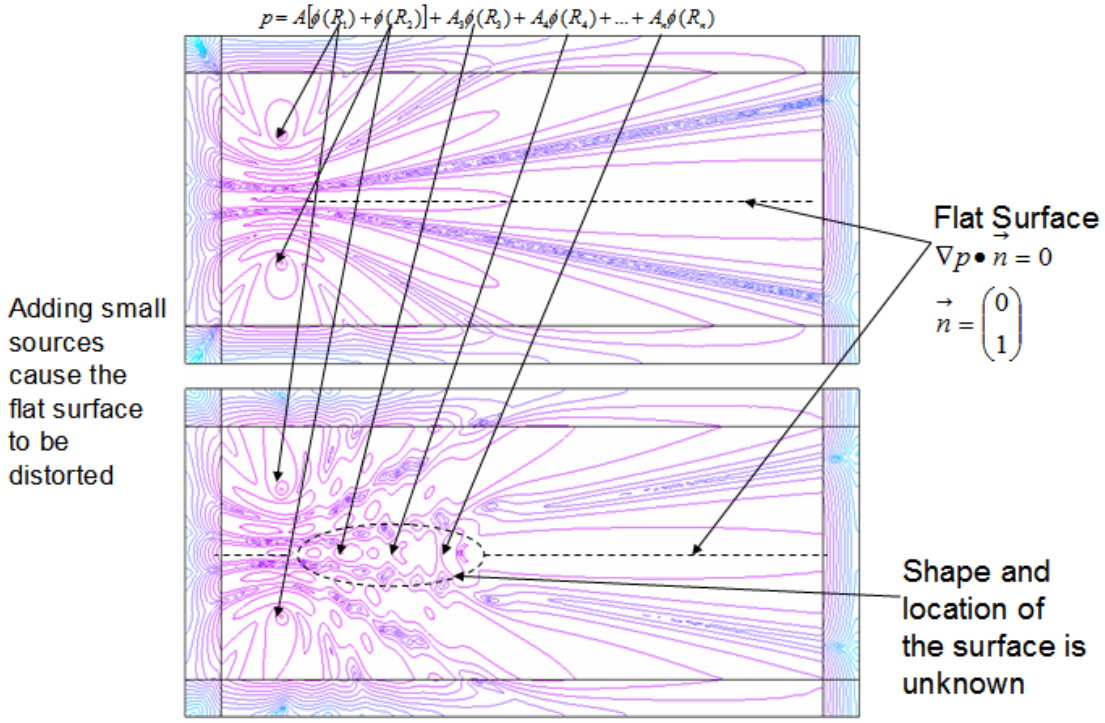

Figure 4.4. Multiple sources make it hard to determine the location of the surface

Consider a grid contain $m \times n$ data points; each point on the grid is a potential point that lies on the surface. A systematic search needs to be conducted to find the point that lies on the surface. Figure 4.5 shows how this search method is conducted. If we let

$y0 - yr$ represent $ymin$, $y0 + yr$ represent $ymax$, Δy be the y-step size, Δx be the x-step size and yr be the distance from the midpoint to $ymin$ or $ymax$, we would start our search at $(x,y0 - yr)$ and move along the y-axis at Δy intervals until we reach $y0 - yr$. We, then, move on to the next point on the x-axis and start the process over again. An outline of the algorithm is given below.

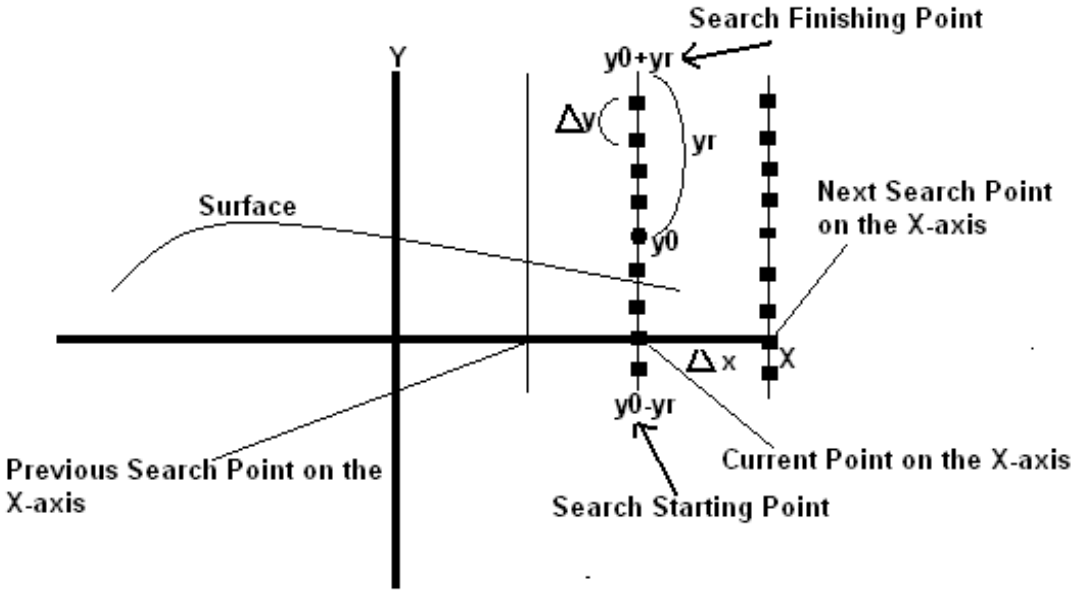

Figure 4.5. Algorithm to find a point on the surface

1- Set the y-step size

2- Set the x-step size

3- Determine the starting and ending point on the y-axis (y_{min} and y_{max})

4- Pick a x-coordinate (x_0) as a starting point

5- Starting at point (x_0, y_{min}), solve for $d(x, y)$ (Equation (4.28))

6- Increment y_{min} by y-step size

7- Repeat step 5 through 7 until the (x_0, y_{max}) is reached

8- Find the point in which $d(x, y)$ change sign. This will be the point in which $d(x, y)$ is closest to zero; thus, it will be a point closest to the surface. In most cases, finding where $d(x, y)$ equals exactly zero is very difficult due to the fact that the y-step size will have to be very small.

9- Increment x_0 by x-step size

10- Repeat step 5 through 9 until the desire distance is reached.

4.5.4 Following the Surface

Finding the surface method discussed in the last section, while effective, can be time consuming and inefficient in many cases. In some cases where a point on the surface is located outside of y_{min} and y_{max}, that point may not be found using the algorithm. In this section, we will discuss another method for finding the surface. In order to follow the surface, we first have to find it. To find that initial starting surface point, we will use steps 1 through 7 of the algorithm discussed in section 4.5.3. Once a point on the surface is found, we can use our algorithm described in the following. We start with $d(x, y)$.

$$d(x, y) = \mathrm{Re}\left(\frac{\partial \phi}{\partial x}\right) \mathrm{Im}\left(\frac{\partial \phi}{\partial y}\right) - \mathrm{Im}\left(\frac{\partial \phi}{\partial x}\right) \mathrm{Re}\left(\frac{\partial \phi}{\partial y}\right) \tag{4.33}$$

We want to follow $d(x, y) = 0$. Finding the null space of $\nabla d(x, y)$ will give the vector tangent to the surface. It is this vector that we want to follow.

1- Find a point (x, y) such that $d(x, y) = 0$

2- Compute $d(x, y)$ at point (x, y)

3- Compute $\nabla d(x, y)$

4- Compute the null-space of $\nabla d(x, y)$

5- Take a small step in the direction of $null\left[\nabla d(x,y)^T\right]$

6- Take the new position and repeat $2-6$.

4.5.5 Simulations

Different simulations were performed. These simulations are discussed in detail in the following sections. Simple models such as a flat surface which requires only two sources were simulated initially followed by more complex systems containing multiple sources.

4.5.6 Surface Modeling Using Acoustic Sources

In section 4.5, we discussed that by placing two sources, one being the actual source and the other being its image, a flat hard surface can be modeled. Here, the main or actual source is placed at $(0,1)$ and its image at $(0,-1)$. They have the same amplitude of 1 and wavenumber of $1\ m^{-1}$. In section 4.5.2, we established that at every point on the hard surface, $d(x,y)$, Equation (4.28), must equal to zero. Thus, plotting a contour of d(x,y)=0 produces a flat hard surface located at midpoint between the main source and its image. This is shown in Figure 4.6.

We can form a hill on the hard surface by using four sources. The main source and it image are placed at locations $(0,1)$ and $(0,-1)$ respectively with an amplitude of 1 and wavenumber of $1\ m^{-1}$. A small source with an amplitude of 0.1 and wavenumber of $1\ m^{-1}$ is placed at $(1,-0.1)$. Another small source with an amplitude of -0.1 and wavenumber of $1\ m^{-1}$ is placed at $(2,0.1)$. The combination of these four sources form a hill on the surface as shown in Figure 4.7.

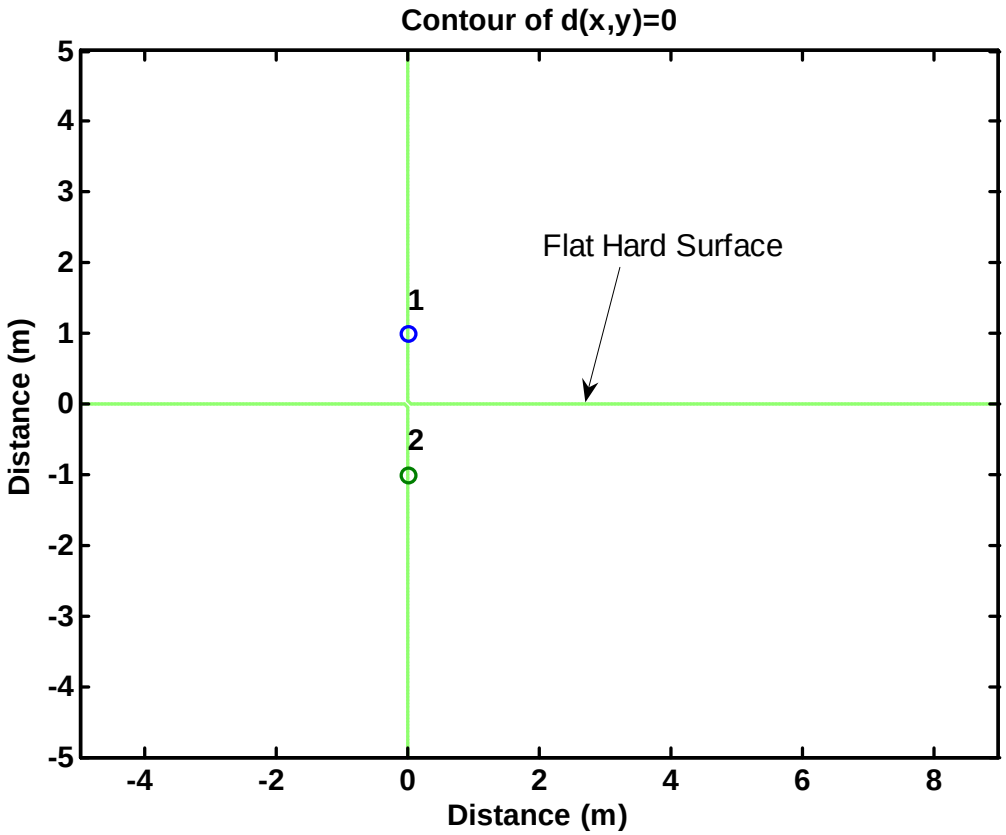

Figure 4.6. Placing two sources at $(0, 1)$ and $(0, -1)$ produces a flat surface

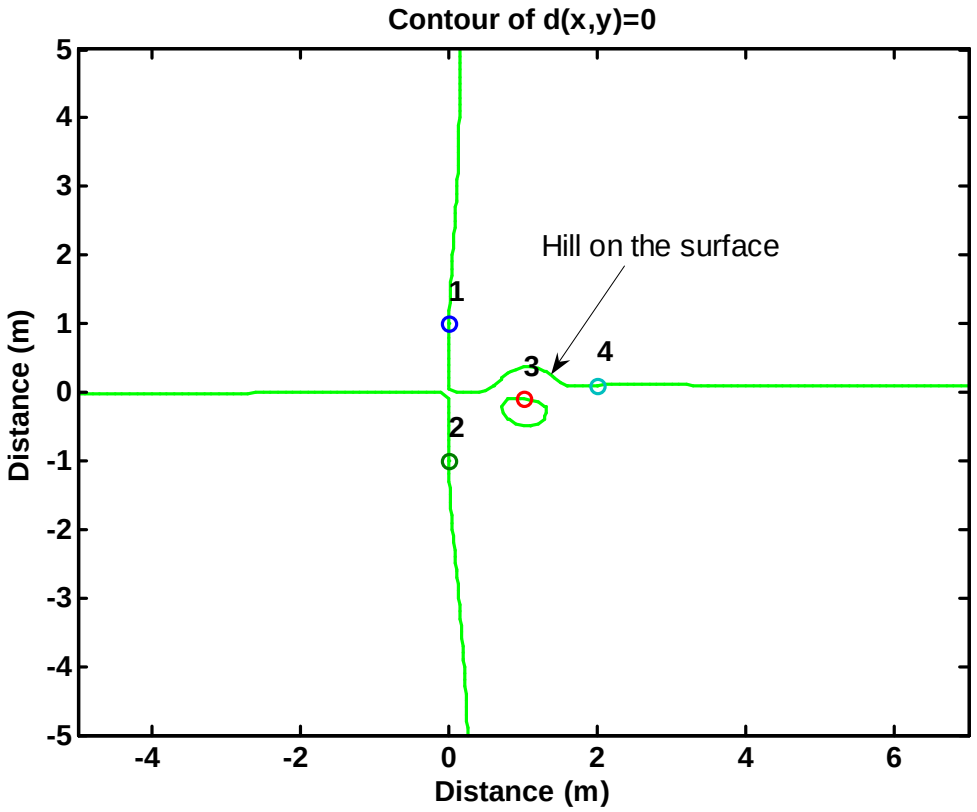

Figure 4.7. Using four sources, a hill can be formed on the hard surface

Now consider a four source system, where two smaller sources are place to the left of the main source and its image. The main source, having an amplitude of 1 and wavenumber of 1 m^{-1}, is placed at $(0, 1)$. Its image, having the same amplitude and wavenumber, is located at (0,-1). Two small sources, one with an amplitude of -0.1 and wavenumber of 1 m^{-1} is placed at $(1, -0.1)$ and another with an amplitude of 0.1 and wavenumber of 1 m^{-1} is placed at $(2, 0.1)$, to form a valley on the hard surface. This is shown in Figure 4.8.

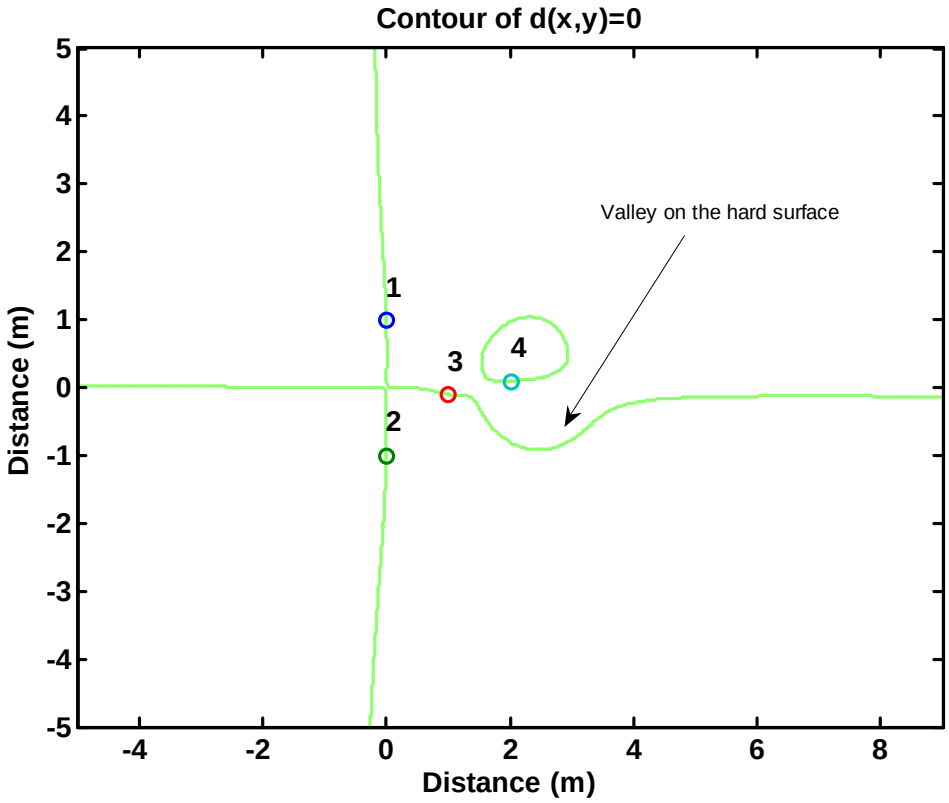

Figure 4.8. Using four small sources will create a valley on the hard surface

Using more than four sources, we can modify a flat hard surface to have both hills and valleys as shown in Figure 4.9. In this case, the main source with an amplitude of

1 and wavenumber of 1 m^{-1} is placed at $(0, 1)$ and its image is placed at $(0, -1)$. In Figure 4.9, these two sources are labeled as 1 and 2 respectively. Six additional sources with the same wavenumber as the main source and various amplitudes are placed to mold the surface into having hills and valleys. Source 3, having an amplitude of -0.1 is placed at location $(1, -0.1)$, source 4 with an amplitude of 0.1 is placed at $(1, 0.1)$, source 5 with an amplitude of -0.1 is placed at $(3, -0.1)$, source 6 with an amplitude of 0.03 is placed at $(4, 0.1)$, source 7 with an amplitude of -0.005 is placed at $(5, -0.1)$ and source 8 with an amplitude of 0.001 is located at $(6, 0.1)$.

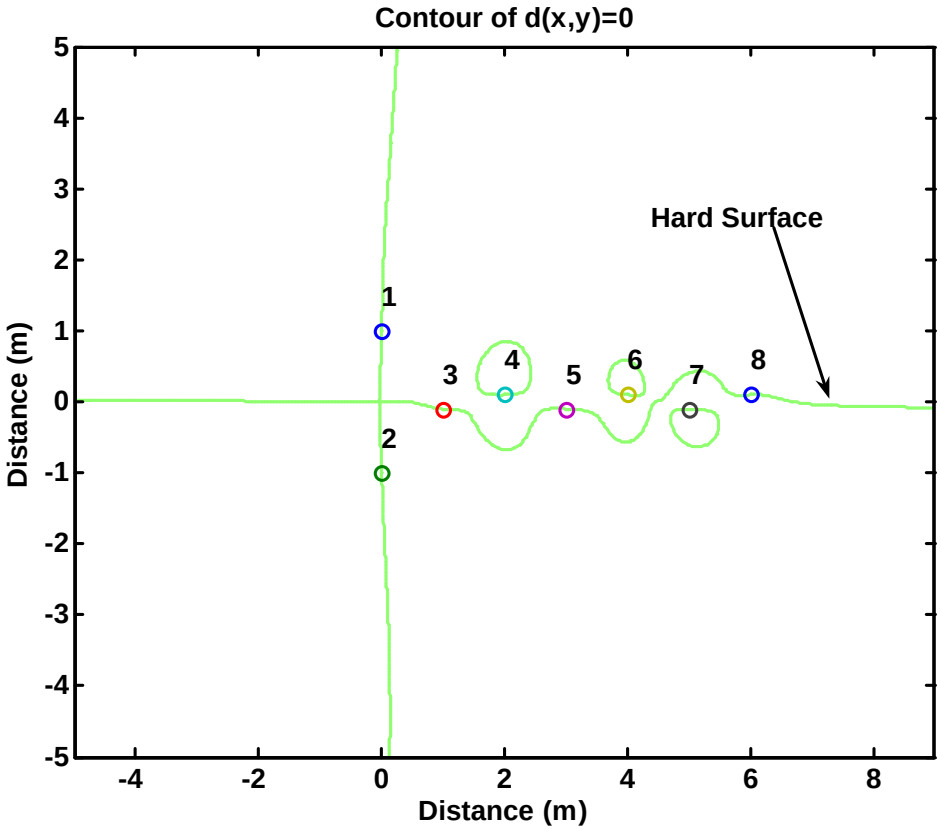

Figure 4.9. Hills and valleys can be formed using multiple sources

4.5.7 Surface Following Algorithm Results

If only the location of a point on the surface is known and the shape of the surface curve is not known, then the surface following algorithm is effective at drawing an outline of the shape of the surface. If a point near the surface is found, it can be used as starting point for the algorithm. Figure 4.10 shows the result of this algorithm. The main source, having an amplitude of 1 and wavenumber of 1 m^{-1}, is located at $(0, 1)$ and its image at $(0, -1)$. Two small sources with amplitudes of -0.1 and 0.1 and wavenumber of 1 m^{-1} are placed at locations $(1, -0.1)$ and $(2, 0.1)$ respectively. The starting point for the algorithm is located approximately at $(7.0, 0.0)$. From this point, the algorithm follows the surface in the negative x-direction and ends approximately $(0.19, 0)$.

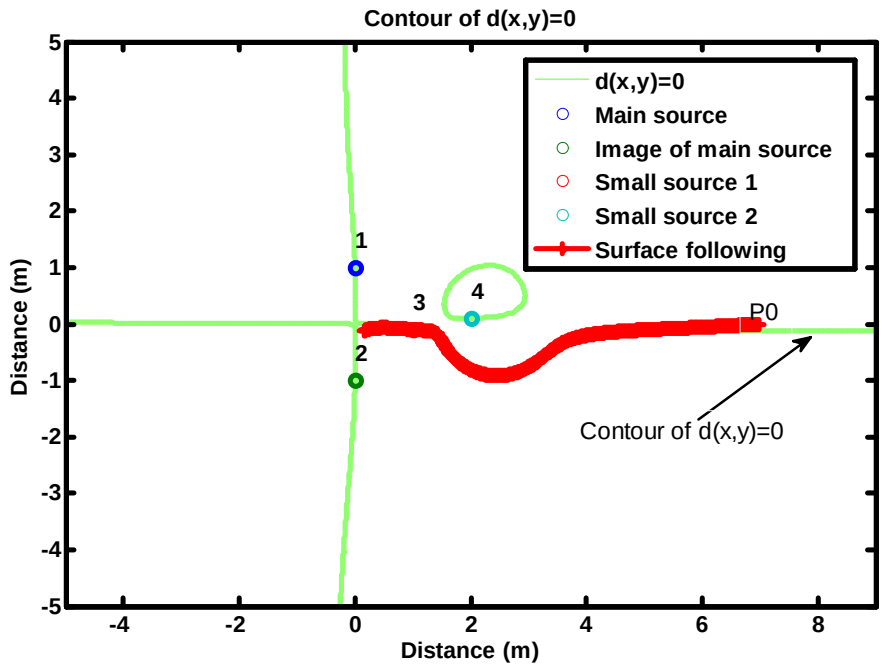

Figure 4.10. The surface following algorithm starting at P0

A slightly more complex surface is shown in Figure 4.11. To form two valleys on the surface, we placed the main source with an amplitude of 1 and wavenumber of 1 m^{-1} at $(0, 1)$ and its image at $(0, -1)$. The main source and its image are labeled as source 1 and 2 in Figure 4.11. Four small sources are placed at locations $(1, -0.1)$, $(2, 0.1)$, $(3, -0.1)$ and $(4, 0.1)$ with amplitudes and wavenumbers of -0.1 and 1 m^{-1}, 0.1 and 1 m^{-1}, -0.1 and 1 m^{-1}, and 0.03 and 1 m^{-1} respectively. These small sources are labeled as source 3, 4, 5 and 6 respectively in Figure 4.11. We choose a point that is close to the surface as a starting point for our algorithm. In this case, that point is located at $(7.4, -0.01)$. The algorithm follows the outline of the surface in the $-x$ direction until it reaches the predetermined destination located at $(0.5, -0.15)$.

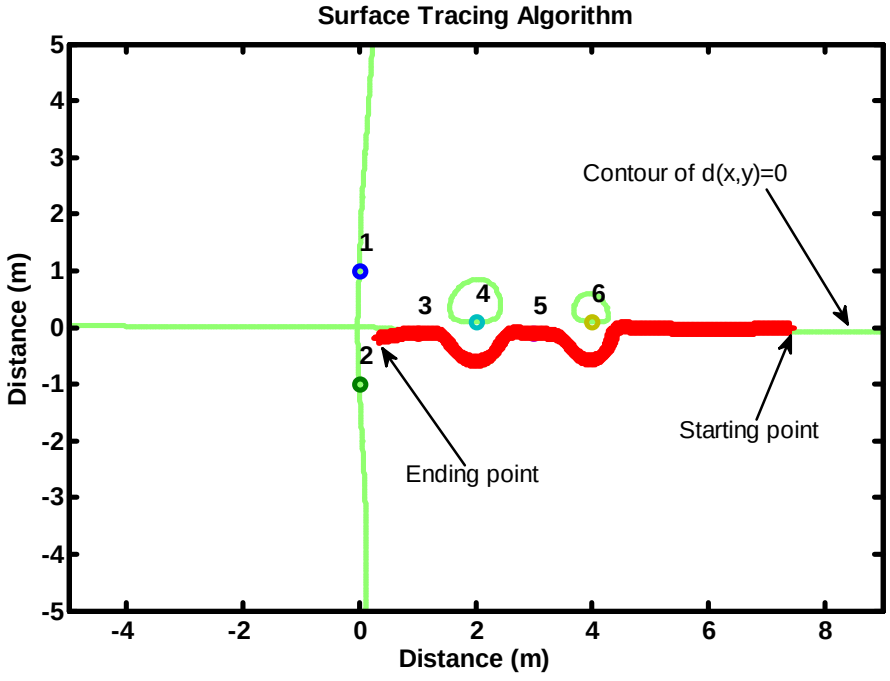

Figure 4.11. Tracing a surface with two valleys

CHAPTER 5

SURFACE GEOMETRY FORMATION USING PERTURBATION

In this chapter, we will investigate the method of using the perturbation theory to estimate the shape of the surface if any of the source parameters (magnitude and phase of the equivalent sources) is changed. For example, if we move an equivalent source from one location to another or if we increase the amplitude of one of the equivalent sources, the shape of the surface will change. There are two problems that we will investigate. The first problem is the forward perturbation problem in which we know the change in source parameters, and we need to find the change in the surface shape. The second problem involves knowing the change in the surface shape, and we need to estimate the change in the source parameters. The second problem will be investigated at a later time.

5.1 Theory

Let D be a function of X at every (x, y) where X is a vector of all optimizing variables.

$$D(X) = \mathrm{Re}\left(\frac{\partial \phi}{\partial x}\right) \mathrm{Im}\left(\frac{\partial \phi}{\partial y}\right) - \mathrm{Im}\left(\frac{\partial \phi}{\partial x}\right) \mathrm{Re}\left(\frac{\partial \phi}{\partial y}\right) \tag{5.1}$$

We rewrite the equation above using a more convenient notation.

$$D(X) = \overset{\bullet}{\phi}_x \hat{\phi}_y - \hat{\phi}_x \overset{\bullet}{\phi}_y \tag{5.2}$$

Let $\varsigma = \eta(x)$ be the solution of $D(X) = 0$. Then, $D(X_0)$ produces $\varsigma = \eta_0(x)$ which is the contour of the surface. If we perturb X_0 by dX then $\eta_0(x)$ may no longer be the solution of $D(X) = 0$. In other words, $D(X_0 + dX)$ evaluated at the previous location of the surface, $\eta_0(x)$, does not equal zero.

$$D(X_0 + dX)|_{\varsigma=\eta_0(x)} \neq 0 \tag{5.3}$$

We define $\widetilde{D}$ as the difference between $D(X_0 + dX)$ and $D(X_0)$ both evaluated at the location of the previous surface, $\eta_0(x)$

$$\widetilde{D} = D(X_0 + dX)|_{\varsigma=\eta_0(x)} - D(X_0)|_{\varsigma=\eta_0(x)}\,. \tag{5.4}$$

Since $D(X_0)|_{\varsigma=\eta_0(x)} = 0$, we have

$$D(X_0 + dX)|_{\eta_0+\delta\eta} = \widetilde{D} \tag{5.5}$$

Where $\delta\eta$=$\eta_1 - \eta_0$.

5.1.1 Perturbation

The perturbation equation is given as

$$\left.\frac{\partial D}{\partial X}\right|_{C_0} dX = -\left.\frac{\partial D}{\partial y}\right|_{C_0} \delta y \tag{5.6}$$

$$\delta y = -\left(\frac{\partial D}{\partial y}\right)^{-1}\left(\frac{\partial D}{\partial X} dX\right) \tag{5.7}$$

$$\frac{\partial D}{\partial y} = -\frac{\partial D}{\partial X}\frac{1}{\delta y} \tag{5.8}$$

Consider a system with many sources, the main source and its image plus small sources. Thus, X, the vector of all optimizing variables is

$$X = [x_i...x_n, y_i...y_n, A_i...A_n, B_i...B_n] \tag{5.9}$$

where x_i is the x-coordinate of the i source, y_i is the y-coordinate of the i source, A_i and B_i are the real and imaginary part of the amplitude of the i source. Substituting Equation (5.9) into the $\frac{\partial D}{\partial X}$ component, we have

$$\left.\frac{\partial D}{\partial X}\right|_{C_0} = \left[\frac{\partial D}{\partial x_i}, ..., \frac{\partial D}{\partial x_n}, \frac{\partial D}{\partial y_i}...\frac{\partial D}{\partial y_n}, \frac{\partial D}{\partial A_i}...\frac{\partial D}{\partial A_n}, \frac{\partial D}{\partial B_i}...\frac{\partial D}{\partial B_n}\right]. \tag{5.10}$$

We multiply Equation (5.10) by the change in the optimizing variables to obtain Equation (5.11).

$$\frac{\partial D}{\partial X}dX = \left[\frac{\partial D}{\partial x_i}, ..., \frac{\partial D}{\partial x_n}, \frac{\partial D}{\partial y_i}...\frac{\partial D}{\partial y_n}, \frac{\partial D}{\partial A_i}...\frac{\partial D}{\partial A_n}, \frac{\partial D}{\partial B_i}...\frac{\partial D}{\partial B_n}\right] \times \begin{bmatrix} \Delta x_i \\ . \\ . \\ . \\ \Delta x_n \\ \Delta y_i \\ . \\ . \\ . \\ \Delta y_n \end{bmatrix} \tag{5.11}$$

$$\frac{\partial D}{\partial y} = \frac{\varepsilon}{u} \tag{5.12}$$

where

$$\varepsilon = D(X_0)|_{\eta_0} - D(X_0 + dX)|_{\eta_1} \tag{5.13}$$

$$u = \Delta y \text{ at every x.} \tag{5.14}$$

5.2 Forward Perturbation

The forward perturbation problem given by the following equation

$$\delta y = -\left(\frac{\partial D}{\partial y}\right)^{-1}\left(\frac{\partial D}{\partial X}dX\right) \tag{5.15}$$

where D is the contour of $d(x, y) = 0$, X is the source parameters, dX is the source perturbation and δy is the surface perturbation. Figure 5.1 illustrates the perturbation concept.

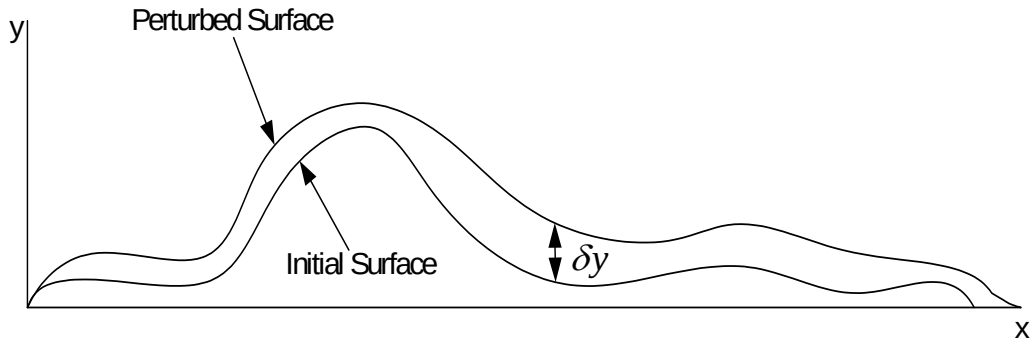

Figure 5.1. Changing the source parameters perturbs the surface geometry

Let dX represent the perturbation of the magnitude and phase of the sources. We define this perturbation as

$$d\Gamma = \{\Delta M_i ... \Delta M_n, \Delta\theta_i ... \Delta\theta_n\}$$

where M_i is the magnitude of the amplitude of the ith source and θ_i is the phase of the ith source.

Consider a system with three sources. The first two sources are the main source and its image. The third source is used to perturb the surface. The initial conditions are given as shown in Table 5.1.

Table 5.1. Source parameters

Source	Wavenumber	Magnitude	Phase (deg)	Location	Comment
1	1	1	0	(0,1)	Main Source
2	1	1	0	(0,-1)	Image of Main Source
3	1	0.0005	90	(10,-0.1)	Small Source

If we perturb the phase of the amplitude of the third source by -90 degrees, then we expect the shape of the surface to change. The location of the new surface can be computed once δy is computed using Equation (5.16). We assign values to the quantities in Equation (5.16) as follows.

$$\begin{aligned} d\Gamma &= \Delta\theta_3 = -90\,\mathrm{deg} \\ \partial\Gamma &= 90\,\mathrm{deg} \\ \partial y &= 0.005m \end{aligned}$$

The above conditions resulted in the waveforms shown in Figure 5.2. The new conditions are tabulated in Table 5.2.

Table 5.2. Source parameters

Source	Wavenumber	Magnitude	Phase (deg)	Location
1	1	1	0	(0,1)
2	1	1	0	(0,-1)
3	1	0.0005	0	(10,-0.1)

5.3 Backward Perturbation

In this section we will investigate the backward perturbation problem. The backward perturbation method will allow for the modification of the contour of the surface to a

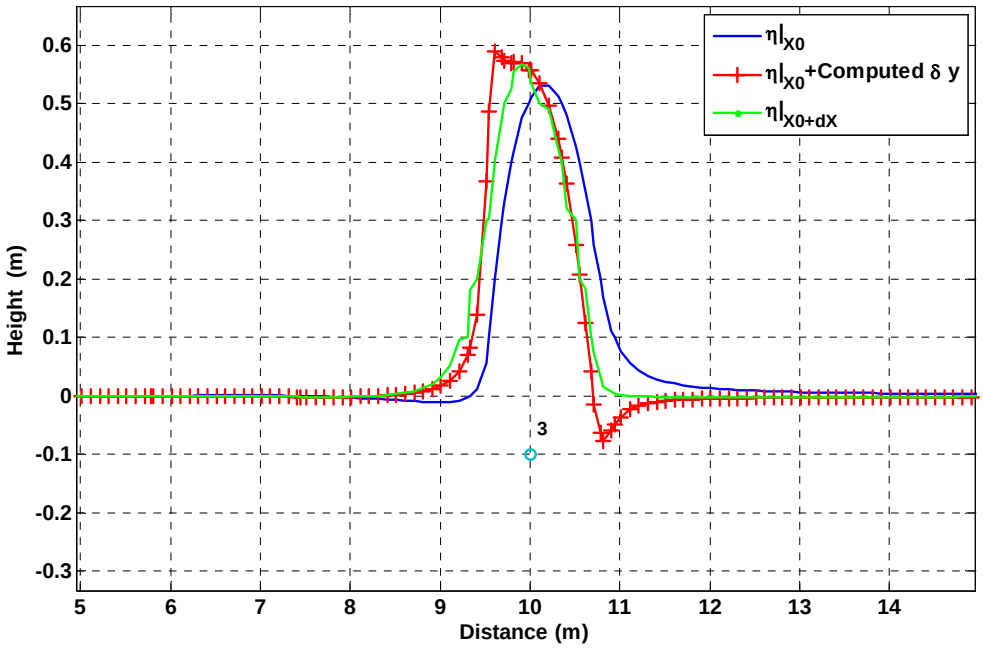

Figure 5.2. The phase of the third source is perturbed by -90 degrees

desired shape. The backward perturbation problem given by the following equation

$$dX = -\left(\frac{\partial D}{\partial y}\delta y\right)\left(\frac{\partial D}{\partial X}\right)^{-1} \tag{5.16}$$

where D is the contour of $d(x, y) = 0$, X is the source parameters, dX is the source perturbation and δy is the surface perturbation. Essentially, since δy is the difference in the y-coordinate of the surface locations and the desired shape, the goal is to minimize δy. This process takes many steps since each step involves perturbing the surface by only a small amount. The results are shown in Figures 5.3, 5.4 and 5.5. We can transform a flat surface into having similar shape as the objective shape in 30 steps.

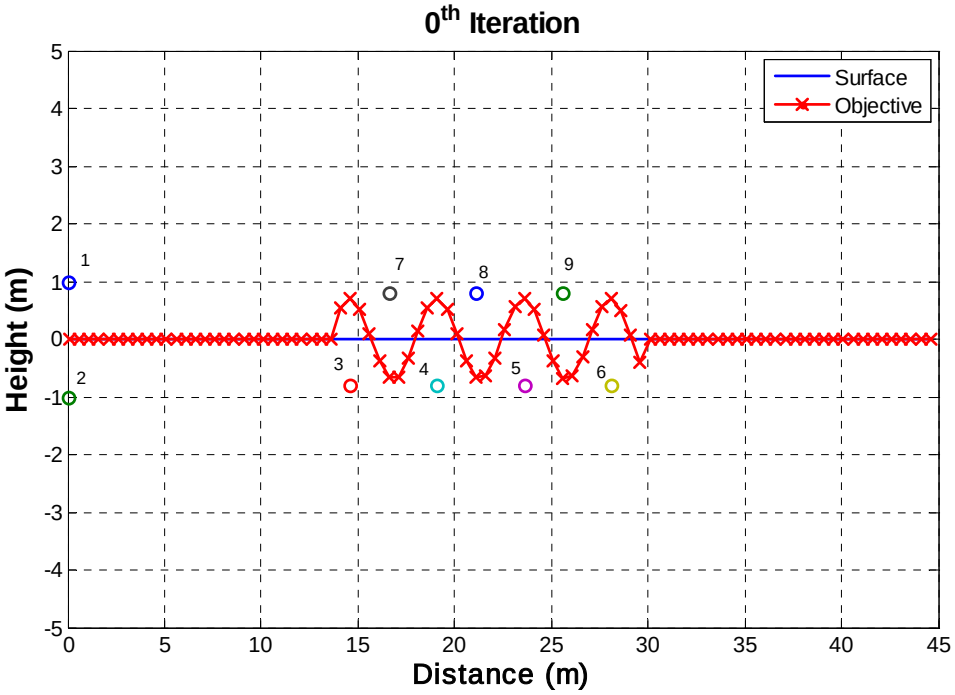

Figure 5.3. The initial surface is flat as shown by the blue line

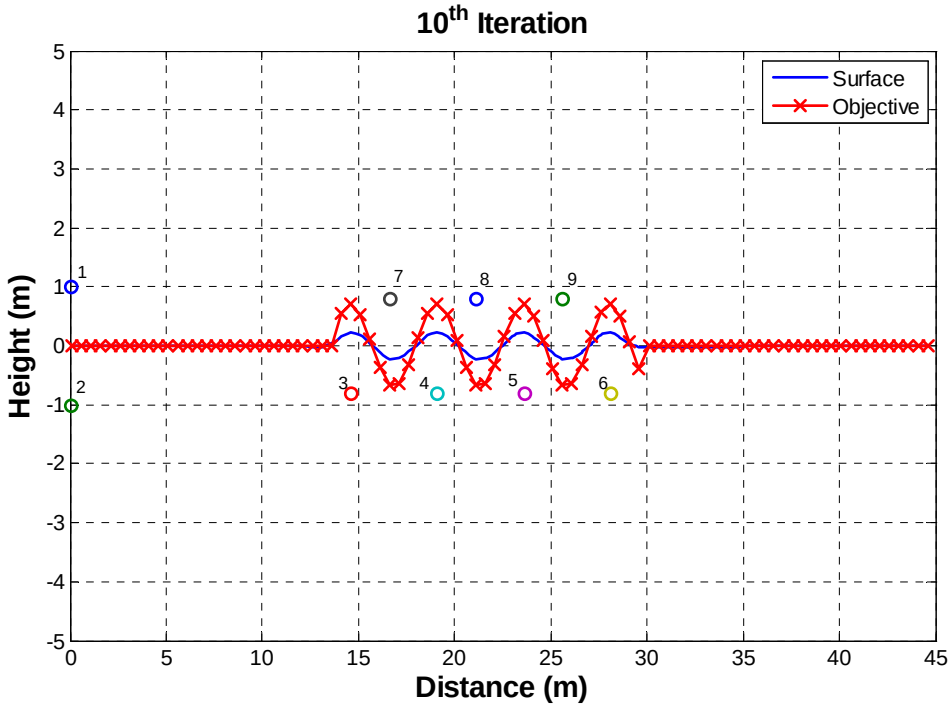

Figure 5.4. After the 10^{th} iteration, small hills and valleys appeared on the surface

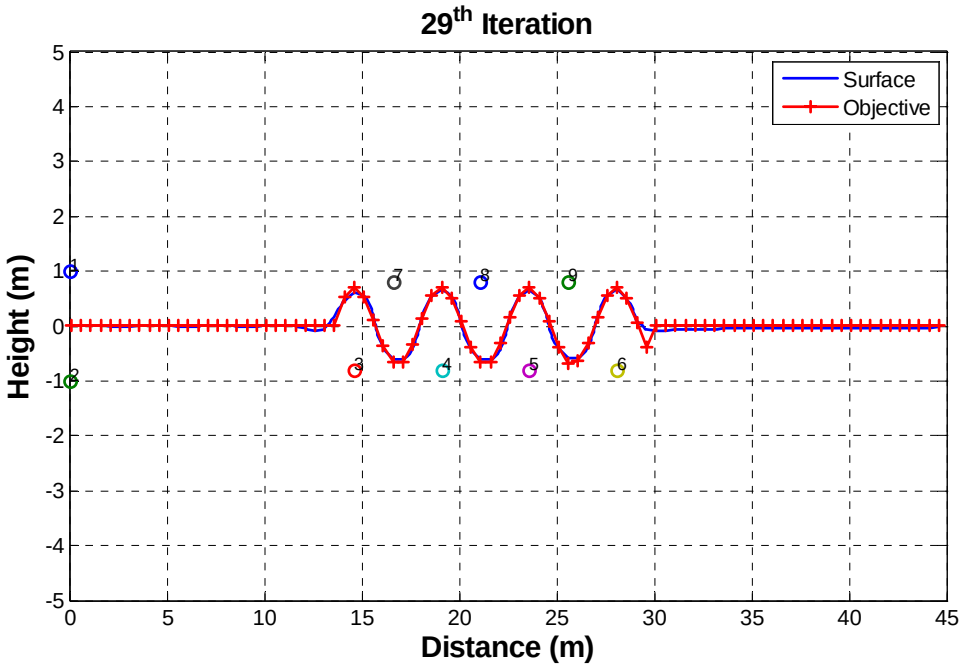

Figure 5.5. After 29 iterations, the surface shape resembles the objective shape

CHAPTER 6

EQUIVALENT SOURCE AMPLITUDE ESTIMATION USING LEAST SQUARES

When constructing a pressure field formed by a radiator of a certain shape using equivalent sources, one of the challenges is the determination of the strengths of the equivalent sources. Other challenges include the placement and number of sources needed to construct the field with minimum error. The strengths or amplitudes of the equivalent sources may be estimated using the least squares method. The least squares method has been used by various researchers to resconstruct extertior and interior acoustic pressure fields [46, 47]. In this chapter, we discuss how the strengths of the equivalent sources are estimated using the least squares method and provide a detailed derivation in the following sections.

6.1 Derivation for Three-Dimensional Problems

For a system containing more than two sources, we rewrite Equation (4.19) as

$$\phi = \sum_{i=1}^{h} \frac{A e^{\mathbf{j}kR_i}}{4\pi R_i} \tag{6.1}$$

Substituting Equation (6.1) into Equation (4.17), we have

$$\nabla \sum_{i=1}^{h} \frac{A_i e^{\mathbf{j}kR_i}}{4\pi R_i} \cdot \overrightarrow{n} = 0 \tag{6.2}$$

We write the above equation as

$$\nabla \left(\frac{A_1 e^{\mathbf{j}kR_1}}{4\pi R_1} + \frac{A_2 e^{\mathbf{j}kR_2}}{4\pi R_2} + ... + \frac{A_h e^{\mathbf{j}kR_h}}{4\pi R_h} \right) \cdot \overrightarrow{n} = 0 \tag{6.3}$$

The first term in Equation (6.3) represents the main source also known as the physical source. Since we know the complex amplitude, A_1, of the main source, we can further rewrite Equation (6.3) as

$$\nabla \frac{A_1 e^{\mathbf{j}kR_1}}{4\pi R_1} \overrightarrow{n} + \nabla \left(\frac{A_2 e^{\mathbf{j}kR_2}}{4\pi R_2} + \frac{A_3 e^{\mathbf{j}kR_3}}{4\pi R_3} + ... + \frac{A_h e^{\mathbf{j}kR_h}}{4\pi R_h} \right) \cdot \overrightarrow{n} = 0 \tag{6.4}$$

The variable A_1 is known and A_2 through A_h are unknowns. We can find A_2 through A_h such that Equation (6.3) would produce an acoustic field equivalent to a specified surface geometry. If the surface geometry is specified (i.e. the objective surface is given), then $\overrightarrow{n}$ is known at every point on the surface. Hence, the only variables left to determine are A_2 through A_h. After a little rearrangement, Equation (6.4) becomes

$$\nabla \left(\frac{A_2 e^{\mathbf{j}kR_2}}{4\pi R_2} + \frac{A_3 e^{\mathbf{j}kR_3}}{4\pi R_3} + ... + \frac{A_h e^{\mathbf{j}kR_h}}{4\pi R_h} \right) \cdot \overrightarrow{n} = -\nabla \frac{A_1 e^{\mathbf{j}kR_1}}{4\pi R_1} \overrightarrow{n} \tag{6.5}$$

Since A_2 through A_h are complex constants and not functions of R, we can rewrite Equation (6.5) as

$$\begin{bmatrix} A_2 & A_3 & ... & A_h \end{bmatrix} \begin{bmatrix} \nabla \frac{e^{\mathbf{j}kR_2}}{4\pi R_2} & \nabla \frac{e^{\mathbf{j}kR_3}}{4\pi R_3} & ... & \nabla \frac{e^{\mathbf{j}kR_h}}{4\pi R_h} \end{bmatrix}^{\mathbf{T}} \cdot \overrightarrow{n} = -\nabla \frac{A_1 e^{\mathbf{j}kR_1}}{4\pi R_1} \overrightarrow{n} \tag{6.6}$$

Writing $n = \overrightarrow{n} = \begin{bmatrix} n_1 & n_2 \end{bmatrix}$, Equation (6.6) becomes

$$\begin{bmatrix} \nabla \frac{e^{\mathbf{j}kR_2}}{4\pi R_2} & \nabla \frac{e^{\mathbf{j}kR_3}}{4\pi R_3} & ... & \nabla \frac{e^{\mathbf{j}kR_h}}{4\pi R_h} \end{bmatrix} \cdot n^{\mathbf{T}} \cdot \begin{bmatrix} A_2 & A_3 & ... & A_h \end{bmatrix}^{\mathbf{T}} = -\nabla \frac{A_1 e^{\mathbf{j}kR_1}}{4\pi R_1} \overrightarrow{n} \tag{6.7}$$

Defining $\Psi_i = \nabla \frac{e^{\mathbf{j}kR_i}}{4\pi R_i}$, Equation (6.7) is rewritten as

$$\left[\begin{array}{cccc} \Psi_2 \cdot n^{\mathbf{T}} & \Psi_3 \cdot n^{\mathbf{T}} & ... & \Psi_h \cdot n^{\mathbf{T}} \end{array} \right] \cdot \left[\begin{array}{cccc} A_2 & A_3 & ... & A_h \end{array} \right]^{\mathbf{T}} = -\Psi_1 \cdot n^{\mathbf{T}} \tag{6.8}$$

For an undulating surface, $\overrightarrow{n}$ will be different from one point on the surface to the next point. Thus, Equation (6.8) will have to be evaluated at the specified points on the surface. Thus,

$$\left[\begin{array}{cccc} \Psi_{21} \cdot n_1^{\mathbf{T}} & \Psi_{31} \cdot n_1^{\mathbf{T}} & ... & \Psi_{h1} \cdot n_1^{\mathbf{T}} \\ \Psi_{22} \cdot n_2^{\mathbf{T}} & \Psi_{32} \cdot n_2^{\mathbf{T}} & ... & \Psi_{h2} \cdot n_2^{\mathbf{T}} \\ . & . & . & . \\ . & . & . & . \\ . & . & . & . \\ \Psi_{2q} \cdot n_q^{\mathbf{T}} & \Psi_{3q} \cdot n_q^{\mathbf{T}} & ... & \Psi_{hq} \cdot n_q^{\mathbf{T}} \end{array} \right] \cdot \left[\begin{array}{cccc} A_2 & A_3 & ... & A_h \end{array} \right]^{\mathbf{T}} = - \left[\begin{array}{c} \Psi_{11} \cdot n_1^{\mathbf{T}} \\ \Psi_{12} \cdot n_2^{\mathbf{T}} \\ . \\ . \\ . \\ \Psi_{1q} \cdot n_q^{\mathbf{T}} \end{array} \right] \tag{6.9}$$

where n is the normal vector at point q on the surface and h is the number of sources. If the number of sources is less than the number of data points on the surface (in other words, $h < q$) then the total number of equations exceeds the total number of unknowns. Hence, we will have an overdetermined system. However, overdetermined systems can be solved reasonably well using the least square method. It is obvious that Equation (6.9) is in the form of $Ma = b$ where M represent the first matrix in Equation (6.9), a represent the second matrix containing the unknown complex amplitudes and b represent the matrix on the right hand side of the equation. Hence,

$$Ma = b \tag{6.10}$$

Using the least square method, we can solve for the a matrix as follows

$$a = \left(M^{\mathbf{H}} M\right)^{-1} M^{\mathbf{H}} b \tag{6.11}$$

6.2 Derivation for Two-Dimensional Problems

The derivation for the 2-D problem is the same as for the 3-D problem with only one difference. The 2-D solution to Equations (4.13), (4.14), (4.15) and (4.16) is different and given as

$$\phi = -A\frac{\mathbf{j}}{4}H_0^{(1)}(kR) \tag{6.12}$$

where $H_0^{(1)}(kR)$ is the order zero Hankel function of the first kind and it's defined as

$$H_0^{(1)}(kR) = J_0(kR) + \mathbf{j}Y_0(kR) \tag{6.13}$$

where $J_0(kR)$ is the bessel function of the first kind and $Y_0(kR)$ is the bessel function of the second kind. We define $\varphi = -\frac{\mathbf{j}}{4}H_0^{(1)}(kR)$ and after going through the same algebra as in the $3-D$ case discussed in section 6.1, we end up with

$$\begin{bmatrix} \varphi_{21}\cdot n_1^{\mathbf{T}} & \varphi_{31}\cdot n_1^{\mathbf{T}} & \dots & \varphi_{h1}\cdot n_1^{\mathbf{T}} \\ \varphi_{22}\cdot n_2^{\mathbf{T}} & \varphi_{32}\cdot n_2^{\mathbf{T}} & \dots & \varphi_{h2}\cdot n_2^{\mathbf{T}} \\ \cdot & \cdot & \cdot & \cdot \\ \cdot & \cdot & \cdot & \cdot \\ \cdot & \cdot & \cdot & \cdot \\ \varphi_{2q}\cdot n_q^{\mathbf{T}} & \varphi_{3q}\cdot n_q^{\mathbf{T}} & \dots & \varphi_{hq}\cdot n_q^{\mathbf{T}} \end{bmatrix} \cdot \begin{bmatrix} A_2 & A_3 & \dots & A_h \end{bmatrix}^{\mathbf{T}} = -\begin{bmatrix} \varphi_{11}\cdot n_1^{\mathbf{T}} \\ \varphi_{12}\cdot n_2^{\mathbf{T}} \\ \cdot \\ \cdot \\ \varphi_{1q}\cdot n_q^{\mathbf{T}} \end{bmatrix} \tag{6.14}$$

Therefore, Equation (6.11) is valid for the $2-D$ case as well.

6.3 Implementation of the Equivalent Source Method

The equivalent source method can be implemented in various computer languages. The flowchart of the algorithm is shown in Figure 6.1. First, the exterior geometry, $\eta(x)$, of the radiator is specified. The focus is of this research is on outdoor noise. Therefore, in this case, the exterior geometry is the geometry of the ground surface. Once the geometry has

been specified, the vector normal to the each point on the surface needs to be calculated. Since we are only interested in the direction of the tangent line, the only information that we need in order to determine the normal vector is the slope at each point on the surface. Computing the null space of a vector parallel to the tangent line will give the normal vector. Thus,

$$\overrightarrow{n} = Null\left(\begin{bmatrix} c & c\frac{\partial \eta}{\partial x} \end{bmatrix}\right) \tag{6.15}$$

where $\frac{\partial \eta}{\partial x}$ is the slope or derivative at point x and c is a positive constant. The equivalent sources may be placed beneath the ground surface. The accuracy of the results depends on the number and locations of the sources. The number and locations of the equivalent sources may differ from one geometry to another. A geometry with many curves may required more sources than one with less curves. Generally, if there are enough sources strategically placed, good results can be obtained. Once the equivalent sources have been placed, the next step is to calculate the amplitudes of these sources. Equation (6.11) represents the least square equation that can be used to estimate the amplitudes.

6.4 Two-Dimensional Results

When the shape of the surface is given, we can find the amplitudes of the small sources such that an equivalent acoustic field can be produced. To accomplish this, we first have to find the vectors that are normal to the surface at the specified points on the surface. The amplitude of the main source may be arbitrary. However, since we chose the source in Comsol to be 10 W, we must find A_1 such that our equivalent main source in Matlab would produce a power of 10 W as well. It turned out that $A_1 = -130.99 - .18221i$ will produce

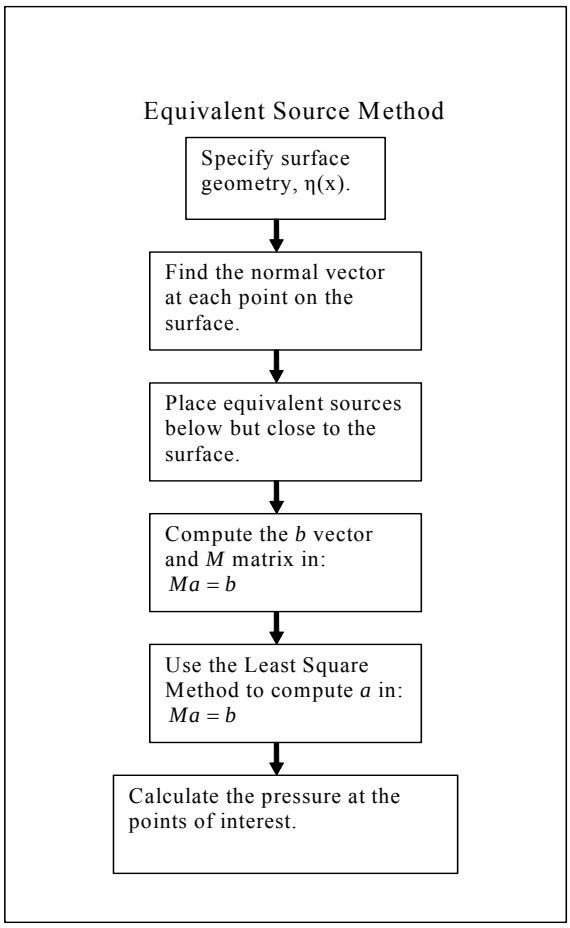

Figure 6.1. Algorithm for calculating the pressure field using the ESM

a source of 10 W. Simulations were done in $2-D$. The surface is shown in Figure 6.2. This surface is replicated in Comsol as shown in Figure 6.4. The excitation frequency is 54.6 Hz which corresponds to the wavenumber of 1 m^{-1}. Figure 6.3 shows the location of the sources. Notice that all the small sources are placed below the surface. Figures 6.5 and 6.6 shows that the results produced by the equivalent source method (ESM) and comsol agree relatively well.

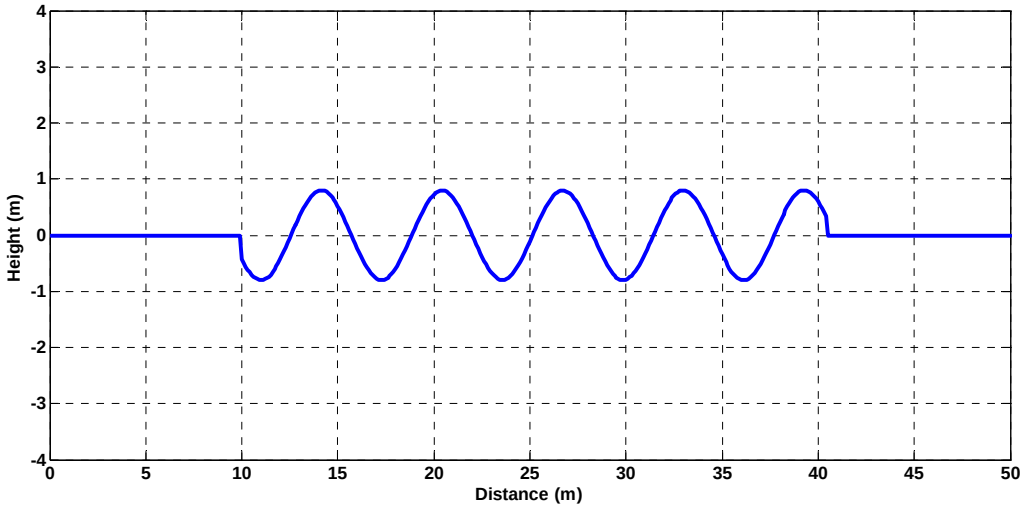

Figure 6.2. The periodic surface defined using Matlab

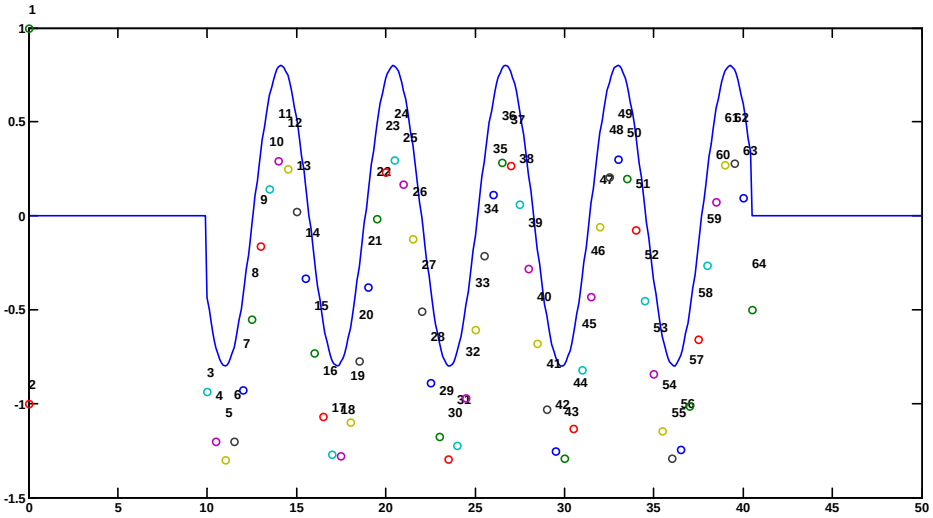

Figure 6.3. At every 0.5 m, there is an equivalent source 0.5 m below the surface

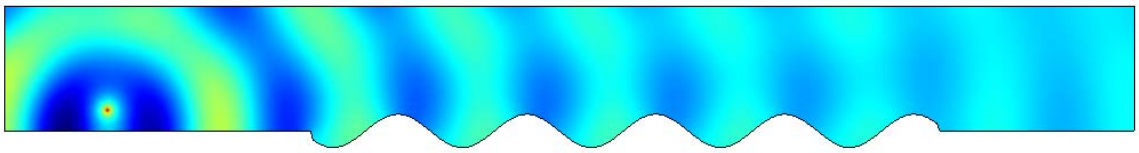

Figure 6.4. Finite element model defined in Comsol Multiphysics

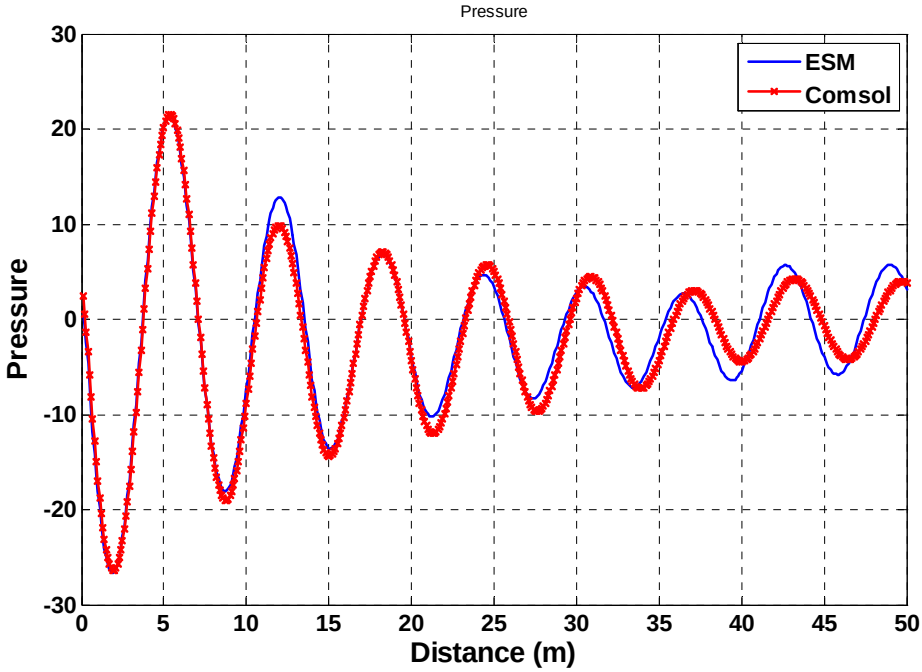

Figure 6.5. Pressure at points $x = 0.1$ m to $x = 50$ m and $y = 1.5$ m

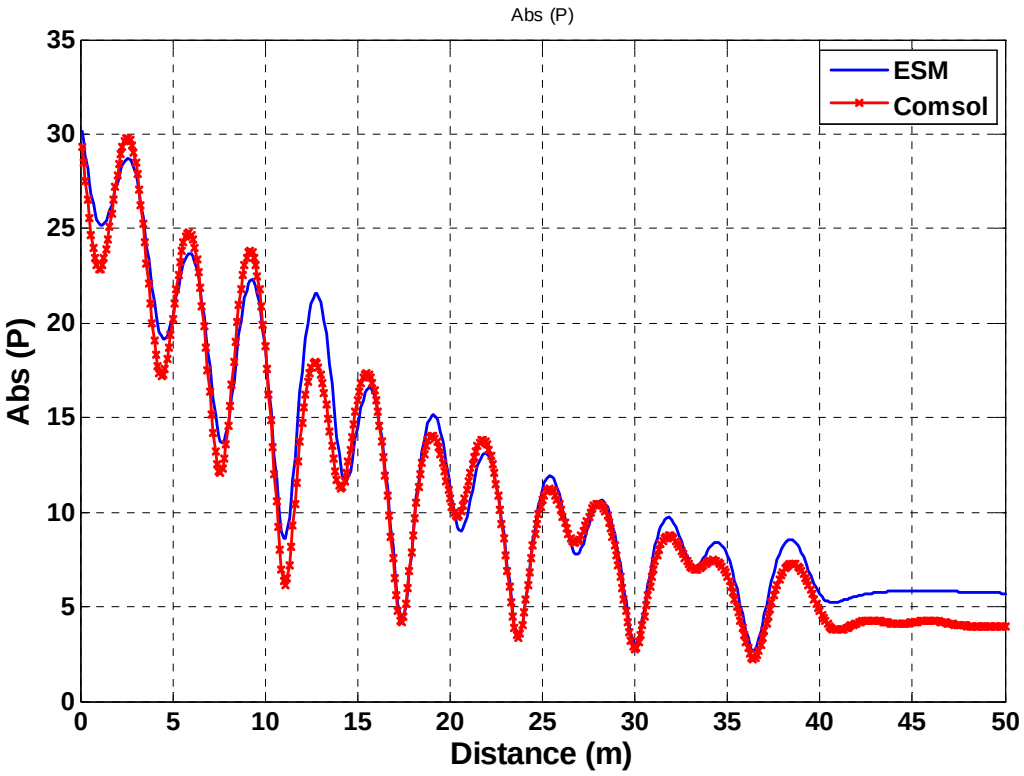

Figure 6.6. Pressure magnitude at points $x = 0.1$ m to $x = 50$ m at $y = 1.5$ m

CHAPTER 7

ACOUSTIC LOSS OPTIMIZATION

In general, a surface with hills, trees and other obstacle results in more acoustic loss than a flat surface. It is intuitive that the higher the hills or the bigger the obstacles the more loss there is. One can design a surface with obstacles so large that most of the acoustic energies simply reflect back toward the source or are dissipated within the obstacles. While it is obvious that this design will result in large losses, it is also not practical. In this section, a method to find a surface that will result in a large loss while practicality is maintained using nonlinear optimization techniques. This is achieved by placing constraints on the size of the hills.

7.1 Theory

Nonlinear optimization techniques can be used to optimize the shape of a surface to produce the most loss. The most successful nonlinear optimization algorithm is the sequential quadratic programming (SQP) algorithm [48]. SQP finds the solution by solving a sequential of quadratic programming subproblems. Our problem is a constrained nonlinear problem as outline below. The objective function or the function to be minimized is $f(x)$,

$$\min f(x) \tag{7.1}$$

subject to the linear inequalities given by

$$Ax \leq b \tag{7.2}$$

Specifically, we want to minimize the absolute value of the pressure, $|\phi|$, at certain locations. We have previously defined ϕ as

$$\phi(x,y) = \frac{Ae^{ikR_1}}{4\pi R_1} + \frac{Ae^{ikR_2}}{4\pi R_2} + \frac{Ae^{ikR_3}}{4\pi R_3} + ... + \frac{Ae^{ikR_n}}{4\pi R_n} \tag{7.3}$$

where

$$R = \sqrt{(x-x_0)^2 + (y-y_0)^2}. \tag{7.4}$$

The first two sources are the main source and its image. Thus, we keep the locations of these two sources constant. Minimizing the pressure at a single location can be misleading. Thus, it is more appropriate to minimize the pressure over a range of positions. We can use line integration to achieve this. Thus, the objective function is defined as

$$f(x) = \Phi(x,y) = \int_{\Omega} |\phi(x,y)| \, d\Omega. \tag{7.5}$$

With Equation (7.5) as the objective function, the total absolute value of the pressure enclosed by the boundary, Ω, is minimized.

7.2 Optimization Procedure

This section discusses the optimization process and provides a basic guideline on choosing basis functions, defining constraints and initial guess. The optimization algorithm is also discussed.

7.2.1 Basis Functions

Prior to running the optimization algorithm, it is important to have a general idea of what the desired surface will look like. While running the algorithm randomly will generate a surface, the shape of that surface may be undesirable or aesthetically unpleasing. If a sinusoidal surface is desired, one may consider using a sinusoidal function as the basis function and its amplitude and wavenumber as the optimizing variables. Using the Gaussian functions as basis functions will unlikely result in a sinusoidal surface. Likewise, if a nonperiodic surface is desired, Gaussian basis functions should be used.

7.2.2 Defining Constraints

The desired shape of the optimal surface is largely determined by the constraints. Consider an undulating surface, the amplitude and the wavelength of the surface are bounded by the constraints. For example, if the amplitude and wavenumber are the optimizing variables, the lower and upper bound of the amplitude can be set to 0.1 and 1.0 m respectively and wavenumber can be set to 0.6283 m^{-1} and 0.1257 m^{-1}. This guarantees that the amplitude of the optimal surface will not exceed 1.0 m, but will be higher than 0.1 m and the wavelength will not be longer than 50 m, but no shorter than 10 m. Similarly, if a nonperiodic surface is desired, Gaussian functions may be used as basis functions. Constraints can be placed on the amplitudes, width and locations of each Gaussian pulse on the $x-$axis. When defining constraints, it is important to keep in mind that while constraints are placed to make sure that the resulted surface is practical, constraints can also limit the loss.

7.2.3 Initial Guess

The initial guess determines the initial geometry of the surface. Different initial guesses may result in different solutions. If one wishes to improve the loss of an existing surface then the existing surface may be used as the initial surface. The optimization algorithm will produce a surface that induces a greater loss unless, of course, the initial surface is already the optimal surface.

7.2.4 Algorithm

The procedure for solving the optimization problem and computing the objective function is shown in Figures 7.1 and 7.2. The optimization procedure begins with a specified initial guess, X_0. X is vector containing the optimization variables, and its representation is different depending on the basis functions used to form the geometry of the surface. For example, if sinusoidal functions are used as the basis functions, X will be a vector consisting of the amplitude, frequency and phase of each sinusoidal waveform. If Gaussian functions are used, X will consist of the width, height and location of each Gaussian pulse.

The next step is to use the ESM to compute the objective function which is the line integral of the absolute value of the pressure between two specified points. This is achieved through placing equivalent sources just below the surface and using the least square method to estimate the amplitudes of these sources. Once this is completed, the pressure field and objective function can be computed. This is shown in detail in Figure 7.2.

Next, the Jacobian of the constraints and Hessian matrix of the Lagrange function are computed. The Jacobian and the Hessian matrix are used to solve the quadratic objective function. After the minimization of the quadratic objective function, a check for

convergence is performed. The conditions for convergence are listed below. If one of these condition is met, then the algorithm has converged.

- The first order optimality conditions are satisfied.
- The search direction ΔX is less than the specified tolerance.

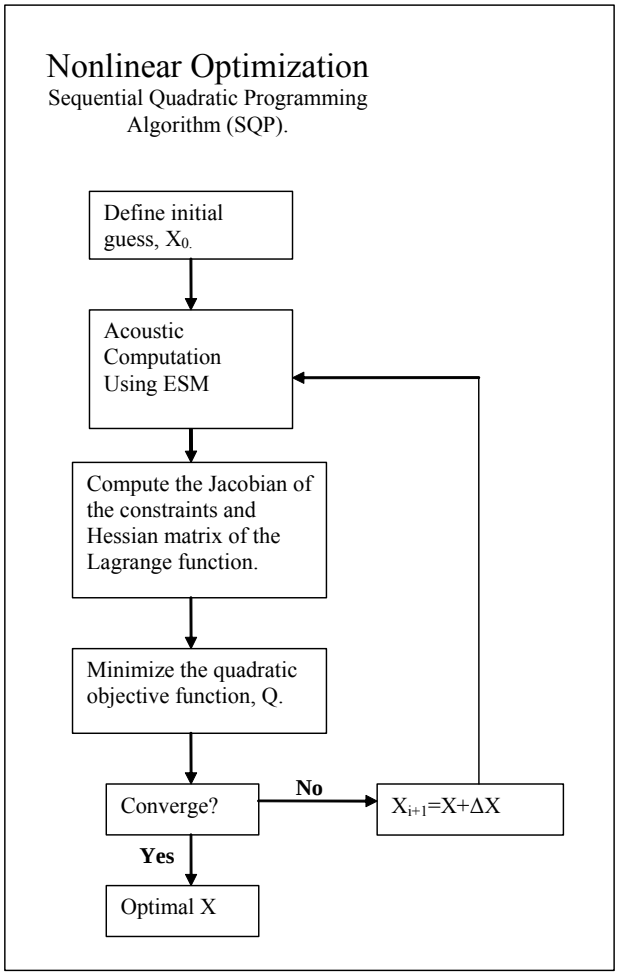

Figure 7.1. Algorithm for acoustic loss optimization using SQP

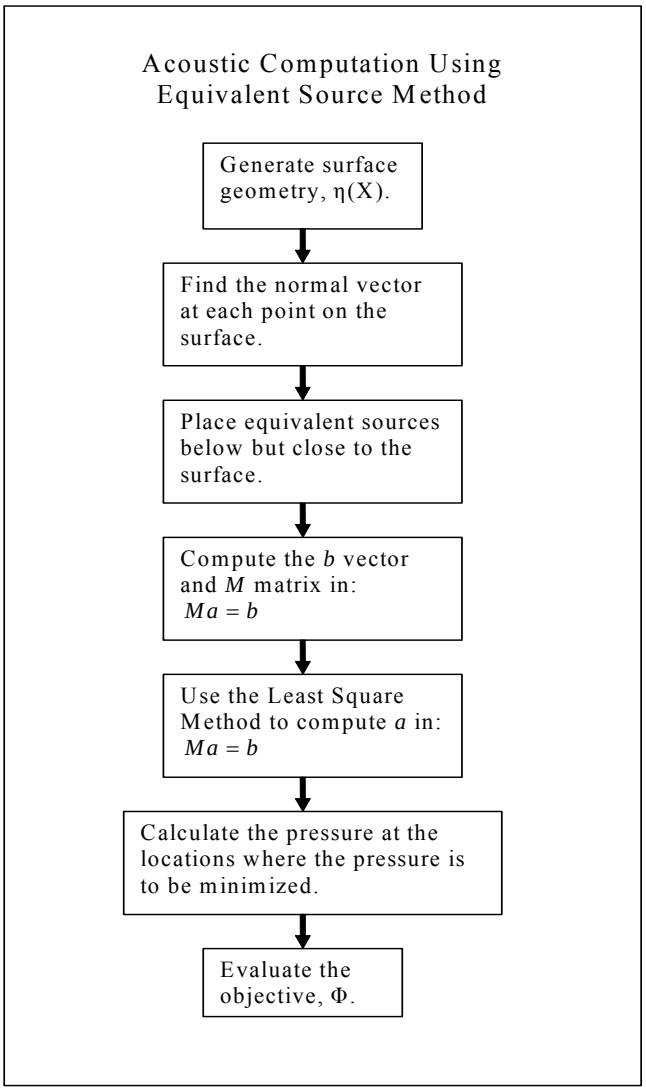

Figure 7.2. Procedure for calculating the objective function

7.3 Wavenumber Optimization Algorithm

In this section, the implementation of the theory discussed in section 7.1 is explored in detail. As previously mentioned, the objective is the maximize the acoustic loss. This can be achieved by finding a surface shape that is capable of suppressing the propagation of the pressure wave for the frequencies of interest. To accomplish this, an arbitrary surface shape that emanates certain pressure field at the area of interest is chosen as the initial surface. This initial surface is periodic with a certain wavenumber. During the optimization, the wavenumber of the surface will change producing a new acoustic field. The pressure within the area of interest will get smaller and smaller as the optimization progresses. The steps for finding the optimal surface wavenumber is listed below.

1- Determine the initial surface shape by specifying the wavenumber.

2- Determine the amplitude of the main source, A_1.

3- Assign an arbitrary value to the amplitude, A_2, of the image of the main source.

4- Define the location and wavenumber of the main source and its image.

5- Define the objective function, $f(x)$.

6- Determine the linear constraints: $Ax \leq b$.

7- Determine the nonlinear constraints if any.

8- Use the equivalent source method to calculate the pressure for the given surface wavenumber.

9- Change the surface wavenumber.

10- Repeat steps 8 and 9 until the desired pressure is obtained.

7.4 Surface Optimization Results

Simulation results are presented in this section. Section 7.4.1 discusses the optimization results for sinusoidal surfaces. Optimization involving surfaces that are not periodic is discussed in Section 7.4.2. Section 7.4.3 presents a setup that results in better improvement.

7.4.1 Sinusoidal Surface Optimization

A arbitrary periodic surface with an amplitude of 0.8 m and a wavenumber of 0.2094 m^{-1} was chosen to be the initial surface which is shown in Figure 7.3. The absolute value of the complex pressure is sampled over the area within the rectangle shown in the figure. We can sum up the absolute values of the complex pressure to get the total pressure within the rectangle and minimizing this total pressure is the objective. Mathematically, the objective function is defined as

$$\Phi = \sum |\phi(x, y)| \tag{7.6}$$

where x and y are the x and y locations where the pressure is measured and k is the wavenumber of the surface. In this particular case, the pressure is measured from $x = 45$ to $x = 50$ at 1 m interval and $y = 1$ to $y = 5$ at 1 m interval. Equation (7.6) is subject to the following constraints,

$$k \leq \frac{2\pi}{\lambda}. \tag{7.7}$$

where λ is the wavelength of the surface. Two constraints are used in this example and are shown below.

$$k \leq \frac{2\pi}{10} \tag{7.8}$$

$$-k \leq -\frac{2\pi}{50} \tag{7.9}$$

The optimal surface is shown in Figure 7.4.

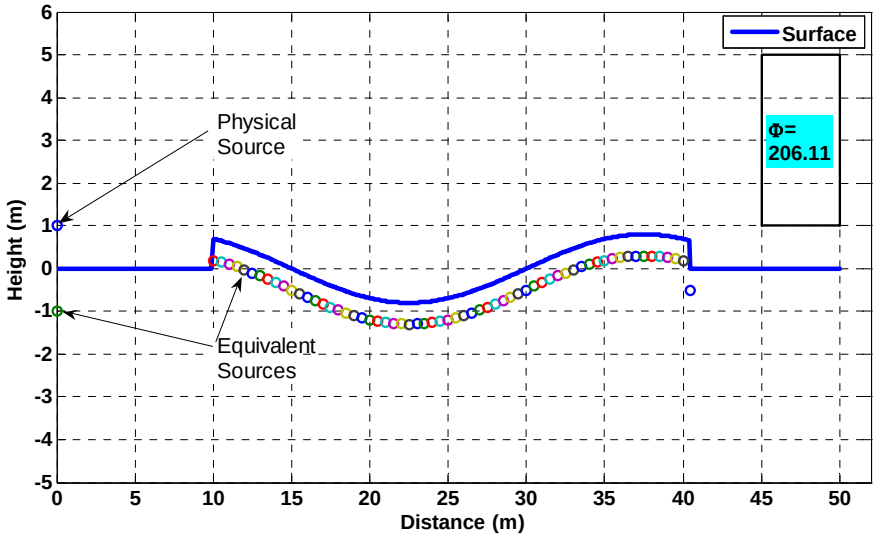

Figure 7.3. The surface before optimization

7.4.2 Non-Sinusoidal Surface Optimization

In this section, we use a set of Gaussian functions as basis functions to construct the surface geometry. Figure 7.5 shows a set of basis functions and the resulting surface. In this simulation, there are 33 Gaussian pulses used. Different surface geometries can be constructed by changing the amplitudes of each of the Gaussian functions.

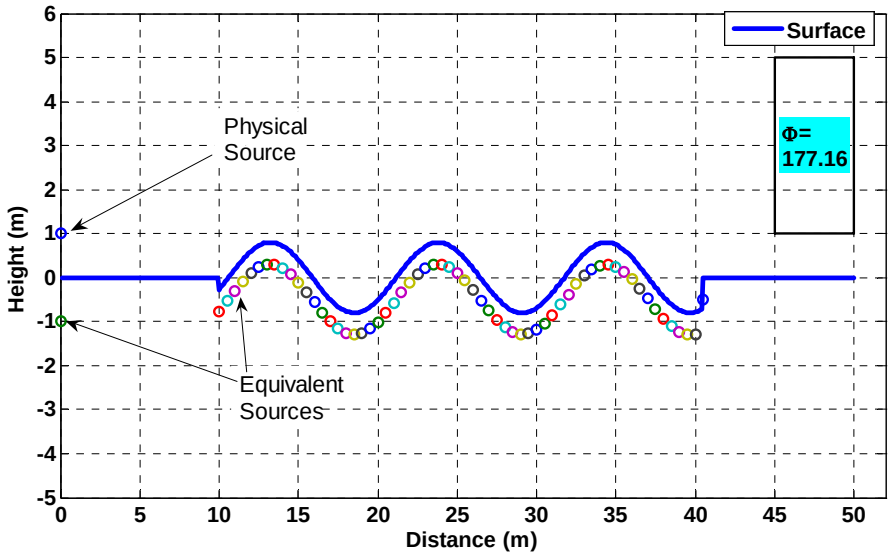

Figure 7.4. The surface after optimization has a wavenumber of 0.5937 $\mathbf{m}^{-1}$

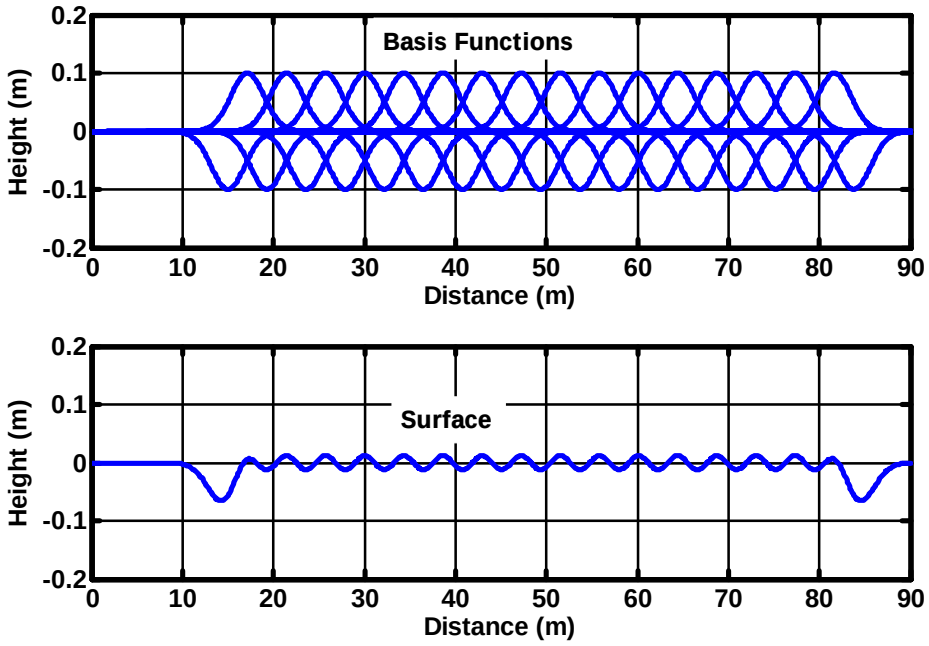

Figure 7.5. Gaussian basis functions and the resulted surface contour

The maximum amplitude of each Gaussian pulse is 1.0 meter; the minimum amplitude of each Gaussian pulse is -1.0 meter. The excitation frequency is chosen as 20Hz. The wavenumber and wavelength of the source are shown below.

$$
\begin{aligned}
k &= \frac{2\pi}{\lambda} \\
k &= \frac{\omega}{c} = \frac{2\pi f}{c} \\
k &= \frac{20\,(2\pi)}{343} \\
k &= 0.3664 m^{-1} \\
\lambda &= \frac{2\pi}{0.3664} = 17m
\end{aligned}
$$

The full width at half maximum (FWHM) of each Gaussian function is 4.3 m. The first pulse is centered at $x = 15$ m. The second pulse is centered at $x = 17.15$ m. Each Gaussian pulse is placed at the interval of 2.15 m apart starting at $x = 15$ m. Initial the Gaussian functions were placed with alternating negative and positive amplitudes as shown in Figure 7.5. Constraints were placed on the amplitudes of the Gaussian functions. These parameters are summarized in the table below.

Table 7.1. Gaussian pulse parameters

Parameter	**Value**
Full Width at Half Maximum (FWHM)	4.3 m
Maximum Amplitude	1.0 m
Minimum Amplitude	-1.0 m
Horizontal position of the first Gaussian pulse	15 m
Interval between pulses	2.15 m
Total number of pulses	33

The amplitude of the main source is set to $-1.3099^2 - i1.8221^{-1}$ which is equivalent to approximately 10 Watts, and located at $(0, 1)$. As mentioned earlier, the frequency of the

main source is 20 Hz. There are a total of 82 equivalent sources used. The amplitudes of these sources are based on the surface geometry and determined using the method discussed in section 6. The first equivalent source which is directly below the main source is placed at $(0, -1)$. The location of the first equivalent source will not change as long as the surface above it remains flat. The remaining 81 sources are placed 0.3 m below the surface at 1.0 m interval starting at $x = 10$ m. Measurements were taken over a square area of 25 m^2 with 5 m in width and 5 m in height. The lower left corner of the square is located at $(90, 1)$. Equation (7.6) is used to compute the total pressure, Φ, inside the square. The results are shown in Figures 7.6 and 7.7. Figure 7.6 shows a relatively flat surface with a total pressure of 162.9 Pa within the measurement area. This flat surface is the initial surface before any optimization is conducted. Figure 7.7 shows the optimized surface with a total pressure of 105.88 Pa within its measurement area. There is an improvement of 57 Pa.

7.4.3 Optimization Setup for Better Loss Improvement

The result of the algorithm depends on many factors including the initial conditions, constraints, placement and number of the equivalent sources. Therefore, it is important that the problem is setup properly to obtain good results. The contraints include the maximum and minimum amplitude of the corrugation, phase of the corrugation and maximum and minimum corrugation wavenumber. A larger loss can be obtained by changing these constraints.

Consider the initial surface shown in Figure 7.8. The surface has an amplitude of 2 meters and undulation length of 180 meters (from $x = 10$ to $x = 190$). The initial wavenumber is 0.1 m^{-1} corresponding to 5.5 Hz. A physical source with 10 watts of power

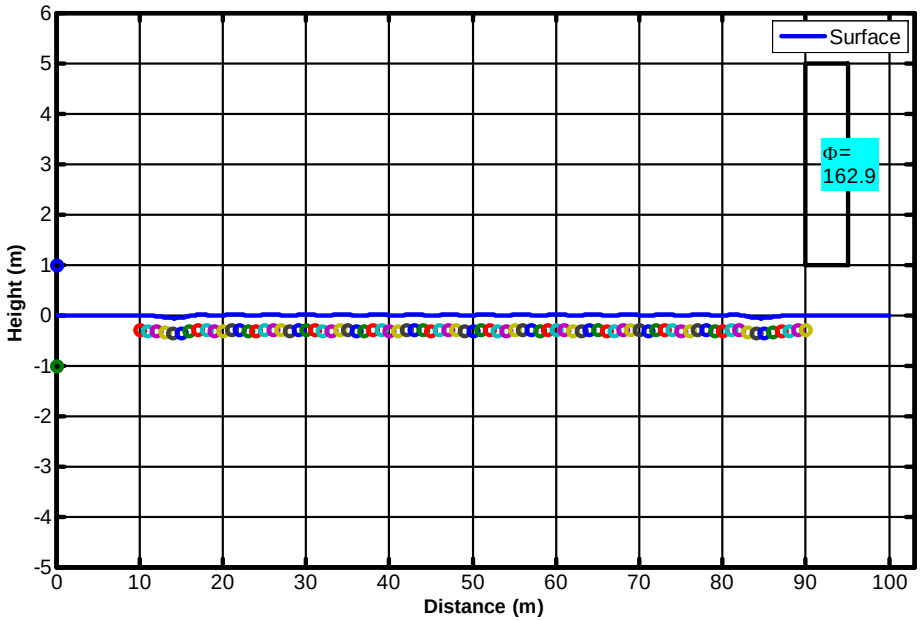

Figure 7.6. Initial surface geometry before optimization

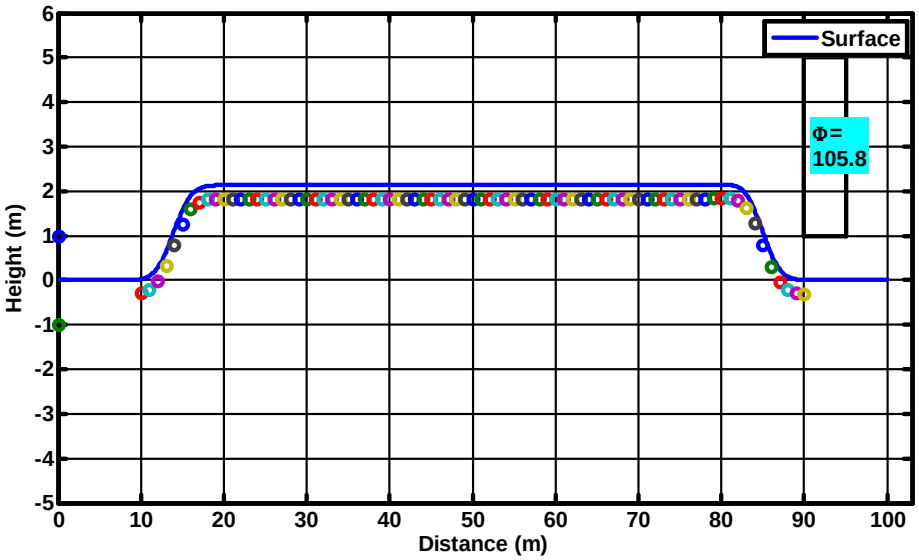

Figure 7.7. The surface geometry after the optimization

and an excitation frequency of 20 Hz is placed at location $(0, 1)$. The total sound pressure level within the area shown by the 4×5 m rectangle was estimated using the equivalent source method and found to be 137 dB with 20 μPa as the reference pressure. A total of 75 equivalent sources including the physical source were used in the computation. Excluding the physical source and its image which are located at $(0, 1)$ and $(0, -1)$ respectively, the equivalent sources are located 0.5 m apart horizontally and 0.5 m below the surface.

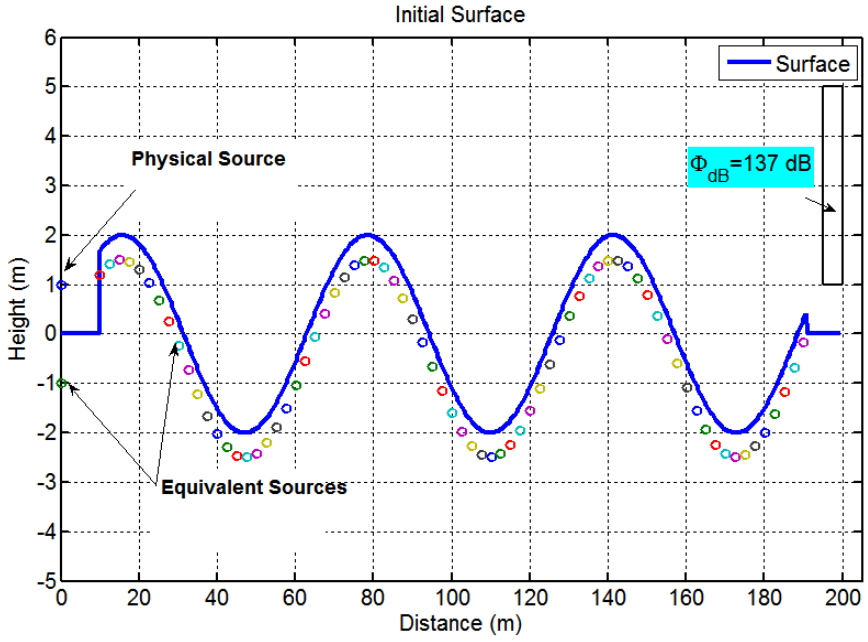

Figure 7.8. Initial surface geometry before optimization

After running the optimization algorithm while keeping the amplitude constant at 2 m, the result is shown in Figure 7.9. The algorithm has adjusted the wavenumber of the surface from 0.1 m^{-1} to 0.4 m^{-1}. The total sound pressure level in the area shown by the rectangle is 127 dB. Although the amplitude of the initial surface and optimized surface are the same, there is an improvement of 10 dB in the model with the optimal surface.

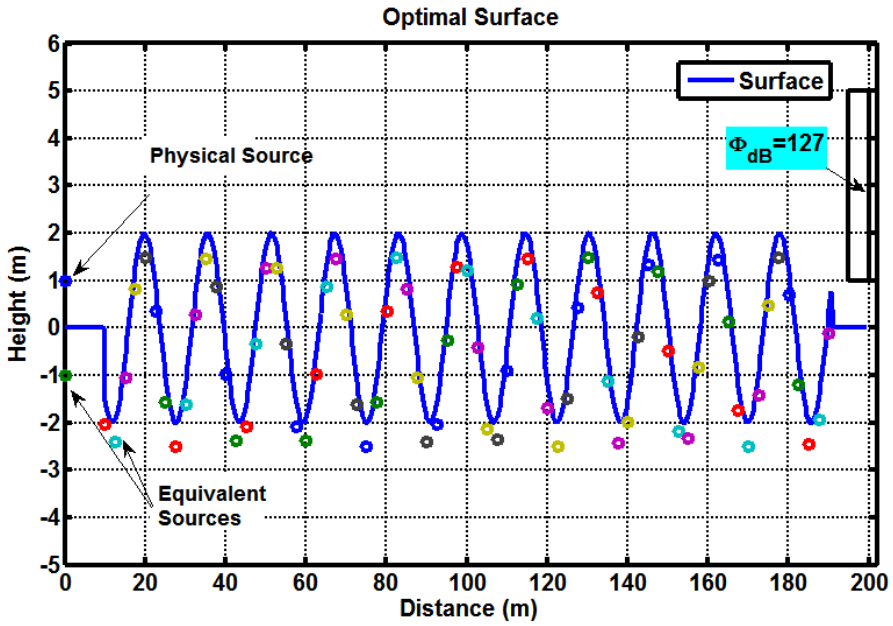

Figure 7.9. Surface geometry after optimization

The surfaces in Figures 7.8 and 7.9 were constructed in Comsol Multiphysics. The simulation result of Comsol model containing the initial surface is shown in Figure 7.10. The Comsol model is surrounded by perfectly matched layers on the sides and top to absorb incoming waves. All other properties remain the same as in the Matlab model. Figure 7.11 shows the Comsol simulation result for the optimal surface. A Comsol and Matlab comparison of the absolute value of the pressure taken from $x = 0$ m to $x = 200$ m and at $y = 3$ m for all x's for the optimal surface is shown in Figure 7.12. A summary of the comparison is shown in Table 7.2.

Table 7.2. Comparison of Comsol Multiphysics and ESM method

Method	Initial Surface Wavenumber	Optimal Surface Wavenumber	Φ_{dB_I}	Φ_{dB_f}
Comsol	0.1 m^{-1}	0.4 m^{-1}	135 dB	127 dB
ESM	0.1 m^{-1}	0.4 m^{-1}	137 dB	127 dB

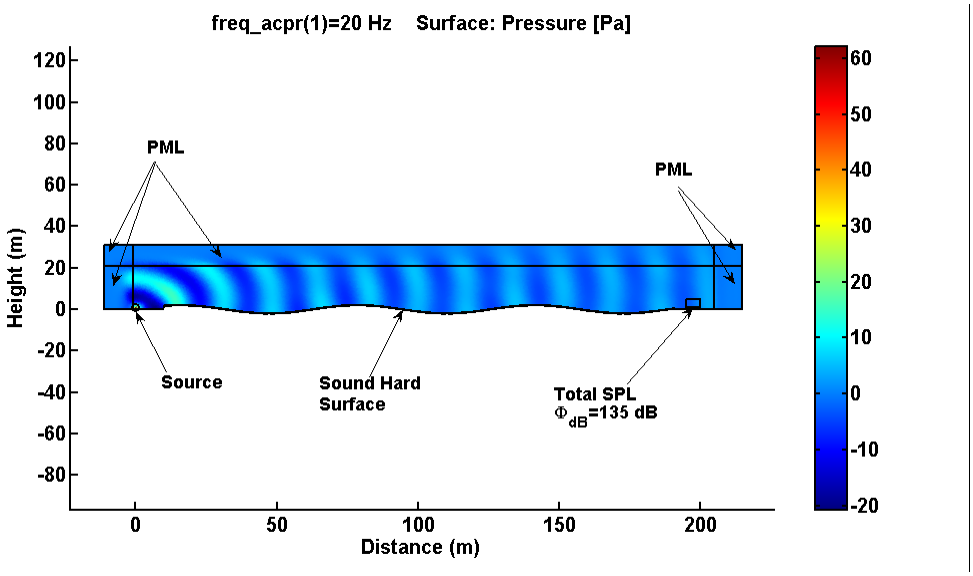

Figure 7.10. Comsol Multiphysics model containing the initial surface

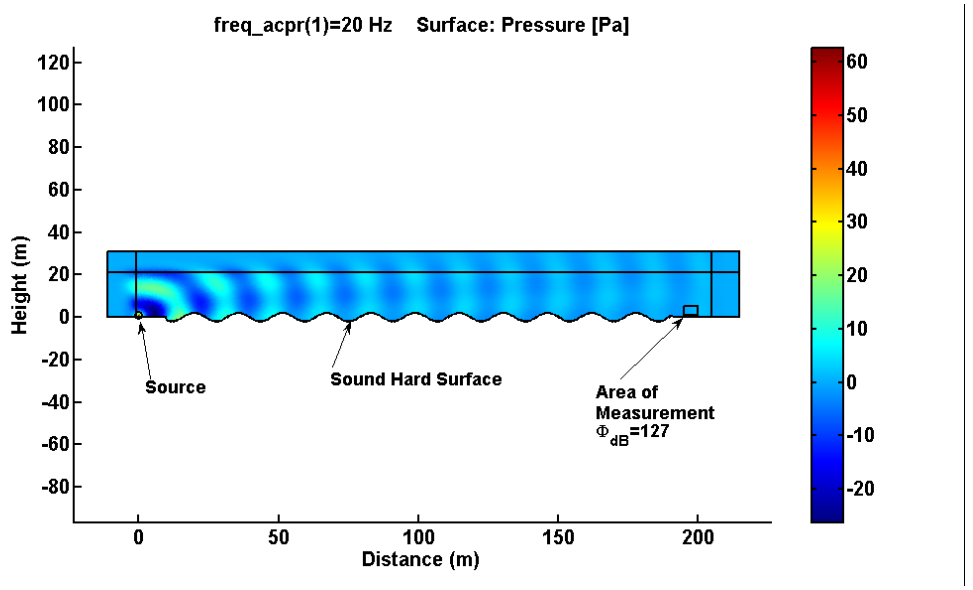

Figure 7.11. Surface after optimization

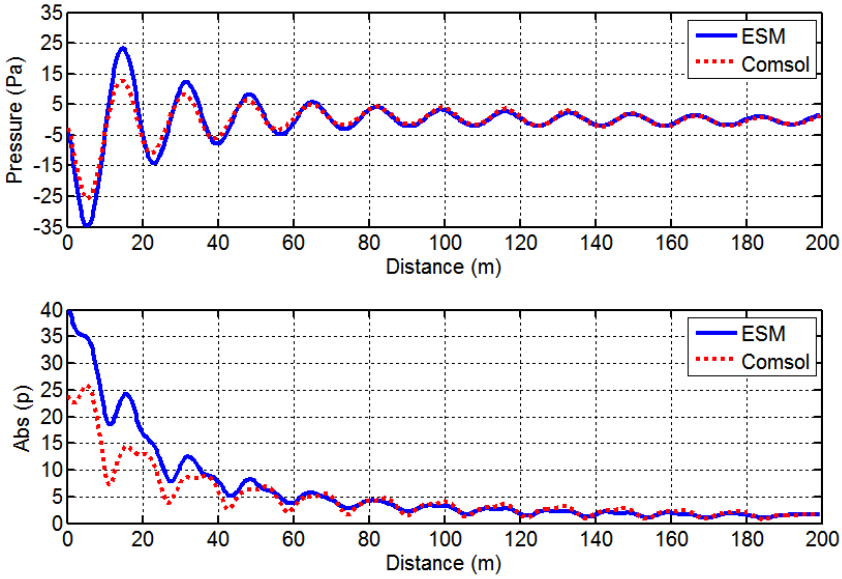

Figure 7.12. Absolute value of the pressure as function of distance (optimal surface)

CHAPTER 8

CONCLUSION

We use finite element simulations to show that an undulating boundary conditions (undulating landscaping) can be used as an effective anti-propagation method to reduce low-frequency outdoor noise. For a corrugation with a wavelength of 3.43 m, amplitude of 2 m and a corrugation length of 82.32 m, the first resonance occurs at 25 Hz. At this frequency, the additional loss due to the undulating boundary is 33.42 dB. We also showed that the undulating landscape create a significant shielding effect at low frequency and close to the ground beyond the landscaping. We show that increasing the corrugation length increases the loss. Changing the amplitude of the corrugation while keeping the length and wavelength of the corrugation constant cause the first resonance frequency to shift. Finally, having phase shifts in the corrugation does not significantly affect the transmission loss in an outdoor environment.

We have discussed the use of equivalent sources to model the effect of hard surfaces on outdoor noise. We derived a mathematical condition and method for locating the surface. We showed that a flat hard surface can be molded into a perturbed quais-flat surface by placing equivalent sources at various distances along the x-axis from the main source. These equivalent sources cause valleys and hills to form on the hard surface, and therefore, can reduce or amplify the noise. We modeled four different surfaces: a flat surface, surface with a hill, surface with a hill and a valley and undulating surface. Our simulations showed

that even though the undulating surface has smaller hills and valleys, it produced the most loss of the four models.

A optimization procedure was developed to compute the surface shape that will result in the most acoustic loss. Due to the simplicity and computational efficiency of ESM, this procedure involves using ESM to compute the acoustic field. The optimization part of the procedure involves using quadratic programming to minimize the loss. The shape of the surface is constructed from a set of basis functions. Sinusoidal and Gaussian basis functions were discussed and results were presented.

BIBLIOGRAPHY

[1] W. E. Baker, *Explosion in Air*, Wilfred Baker Engineering, San Antonio, TX, 1983.

[2] M. Y. H. Bangash, *Impact and Explosion*: *Analysis and Design*, CRC Press, Boca Raton, FL, 1993.

[3] R. D. Ford, D. J. Sounders, and G. Kerry, "The acoustic pressure waveform from small unconfined charges of plastic explosive," *J. Acoust. Soc. Am.* 94, 408-417 (1993).

[4] W. Reed, "Atmospheric attenuation of explosion waves," *J. Acoust. Soc. Am.* 61, 39-47 (1977).

[5] M. J. Downing, K. L. Gee, C. M. Hobbs, M. M. James, and V. W. Sparrow, "Measurement and prediction of nonlinearity of outdoor propagation of periodic signals," *J. Acoust. Soc. Am.* 120, 2491-2499 (2006).

[6] F. Walkden and M. West, "Prediction of enhancement factor for small explosive sources in a stratified moving atmosphere," *J. Acoust. Soc. Am.* 84, 321-326 (1988).

[7] R. H. Lyon, "Noise reduction of rectangular enclosures with one flexible wall," *J. Acoust. Soc. Am.* 35, 1791–1797 (1963).

[8] P. M. Morse, "Transmission of sound through a circular membrane in a plane wall," *J. Acoust. Soc. Am.* 40, 354–366 (1966).

[9] S-M. Kim and Y-H. Kim, "Structural-acoustic coupling in a partially opened plate-cavity system: Experimental observation by using nearfield acoustic holography," *J. Acoust. Soc. Am.* 109, 65-74 (2001).

[10] P. Schomer and A. Averbuch, "Indoor human response to blast sounds that generates rattles," *J. Acoust. Soc. Am.* 82, 665-673 (1989).

[11] P. D. Schomer, E. Buchta and K-W. Hirch, "Decibel annoyance reduction of low-frequency blast attenuating windows," *J. Acoust. Soc. Am.* 89, 1708-1713 (1991).

[12] L. Liu and D. G. Albert, "Acoustic pulse propagation near a right-angle wall," *J. Acoust. Soc. Am.* 119, 2073-2083 (2006).

[13] Y. Kluizenaar et al., "Urban road traffic noise and annoyance: The effect of a quiet facade," *J. Acoust. Soc. Am.*, 130, 1936-1942 (2011).

[14] Z. Mackawa, "Noise reduction by screens," *Appl. Acoust.,* vol. 1, 157-173 (1968).

[15] D. J. Saunders and R. D. Ford, “A study of the reduction of explosive impulses by finite sized barriers,” *J. Acoust. Soc. Am.* 94, 2859–2875 (1993).

[16] U. J. Kurze, “Noise reduction by barriers," *J. Acoust. Soc. Am.* 55, 504-518 (1974).

[17] T. Isei, T. F. W. Embleton, and J. E. Piercy, “Noise reduction by barriers on finite impedance ground," *J. Acoust. Soc. Am.* 67, 46-58, (1980).

[18] A. I. Papadopoulos, and C. G. Don, “A study of barrier attenuation by using acoustic impulses," *J. Acoust. Soc. Am.* 90, 1011-1018 (1991).

[19] M. Vang and M. Bikdash, "Simulation Study of Low-Frequency Outdoor Noise Reduction Using Undulating Landscaping," *IEEE SoutheastCon 2009*, 416-421 (2009).

[20] T. Kundu, S. Banerjee and K. V. Jata, "An experimental investigation of guided wave propagation in corrugated plates showing stop bands and pass bands," *J. Acoust. Soc. Am.* 120, 1217-1226 (2006).

[21] M. Ochmann, "The complex equivalent source method for sound propagation over an impedance plane," *J. Acoust. Soc. Am.* 116, 3304-3311 (2004).

[22] C-X. Bi, X-Z. Chen and J. Chen, "Sound field separation technique based on equivalent source method and its application in nearfield acoustic holography," *J. Acoust. Soc. Am.* 123, 1472-1478 (2008).

[23] J. S. Bradley and J. A. Birta, “On the sound insulation of wood stud exterior walls," *J. Acoust. Soc. Am.* 110, 3086-3096 (2001).

[24] Lord Raleigh, *The Theory of Sound.* Macmillan and Co., London, vol. 2, 1929.

[25] H. Feshbach and A. M. Clogston, “Perturbation of Boundary Conditions," *Physical Review*, vol. 9, 89-94 (1941).

[26] O.R. Asfar and A.H. Nayfeh, "Circular Waveguide with Sinusoidally Perturbed Walls," *IEEE Transactions on Microwave Theory and Techniques*, vol. 23, 728-734 (1975).

[27] O.R. Asfar and M.A. Hawwa, "Coupled-mode analysis of Love waves in a filter film with periodically corrugated surfaces," *Transactions on Ultrasonics, Ferroelectrics and Frequency Control, IEEE,* vol. 41, 13 - 18 (1994).

[28] O.R. Asfar, A. Hussein and A. Ijjeh, "Application of the fundamental matrix method for two-point boundary-value problems to mode coupling in a parallel-plate waveguide having multiperiodic wall corrugations," *IEEE Transactions on Magnetics,* vol. 25, 2989 - 2991 (1989).

[29] U.F. Kristiansen and G.A. Wiik, "Experiments on sound generation in corrugated pipes

with flow," *J. Acoust. Soc. Am.* 121, 1337–1344 (2007).

[30] M.K Law, K.M. Li and C.W. Leung, "Noise reduction in tunnels by hard rough surfaces," *J. Acoust. Soc. Am.* 124, 961–972 (2008).

[31] J. A. DeSanto, "Scattering from a Periodic Corrugated Structure: Thin Comb with Soft Boundaries," *J. Math Phys*., vol. 12, 1913–1921 (1971).

[32] O.R. Asfar, "A Novel Narrowband Waveguide Filter," *IEEE Antennas and Propagation Society International Symposium*, vol. 4, 2526 - 2529 (1997).

[33] P. Boulanger et al., "Ground effect over hard rough surfaces," *J. Acoust. Soc. Am.* 104, 1474-1482 (1998).

[34] C. Potel et al., "Lamb wave attenuation in a rough plate. II. Analytical and numerical results in a fluid plate," *Journal of Applied Physics*, vol. 104, 2008.

[35] J.A. Fawcett, "A scattering-chamber approach for solving finite rough surface scattering problems," *J. Acoust. Soc. Am.* 118, 1348–1357 (2005).

[36] G. H. Koopmann, L. Song and J. B. Fahnline, "A method for computing acoustic fields based on the principle of wave superposition," *J. Acoust. Soc. Am*. 86, 2433-2438 (1989).

[37] L. Song, G. H. Koopman, and J. Fahnline, "Numerical errors associated with the method of superposition for computing acoustic fields," *J. Acoust. Soc. Am.* 89, 2625–2633 (1991).

[38] R. Jeans and I. C. Mathews, "The wave superposition method as a robust technique for computing acoustic fields," *J. Acoust. Soc. Am*. 92, 1156-1166 (1992).

[39] M. E. Johnson, S. J. Elliott, K-H. Baek, and J. Garcia-Bonito, "An equivalent source technique for calculating the sound field inside an enclosure containing scattering objects," *J. Acoust. Soc. Am.* 104, 1221-1231 (1998).

[40] P. A. Nelson and S. H. Yoon, "Estimation of acoustic source strength by inverse methods: part I, conditioning of the inverse problem," *Journal of Sound and Vibration*, vol. 233, issue 4, 639-664 (2000).

[41] P. A. Nelson and S. H. Yoon, "Estimation of acoustic source strength by inverse methods: part II, experimental investigation of methods for choosing regularization parameters ," *Journal of Sound and Vibration*, vol. 233, issue 4, 665-701 (2000).

[42] M. E. V. Pinho and J. R. Arrudo, "On the use of the equivalent source method for nearfield acoustic holography," *ABCM Symposium Series in Mechatronics*, vol. 1, 590-599 (2004).

[43] L. Bouchet, T. Loyau, N. Hamzaoui and C. Boisson, "Calculation of acoustic radiation using equivalent-sphere methods," *J. Acoust. Soc. Am*. 107, 2387-2397 (2000).

[44] M. Hornikx and J. Forssen, "The 2.5-dimensional equivalent sources method for directly exposed and shielded urban canyons," *J. Acoust. Soc. Am.* 122, 2532-2541 (2007).

[45] P. Filippi , A. Bergassoli, D. Habault and J.P. Lefebvre, *Acoustics: Basic Physics, Theory, and Methods*, Academic Press, San Diego, 1999.

[46] Z. Wang and S. F. Wu, "Helmholtz equation-least-squares method for reconstructing the acoustic pressure field," *J. Acoust. Soc. Am*. 102, 2020–2032 (1997).

[47] S.F. Wu and J. Yu, "Reconstructing interior acoustic pressure fields via Helmholtz equation least-squares method," *J. Acoust. Soc. Am*. 104, 2054–2060 (1998).

[48] J-L Hu, Z. Wu, H. McCann, L E Davis and C-G Xie, "Sequential Quadratic Programming Method for Solution of Electromagnetic Inverse Problems," *IEEE Transaction on Antennas and Propagation*, vol. 53, no. 8 (2005).